Lithos 320–321 (2018) 567–582

Contents lists available at ScienceDirect

Lithos

journal homepage: www.elsevier.com/locate/lithos

The origin of magnetite-apatite rocks of Mushgai-Khudag Complex, South Mongolia: mineral chemistry and studies of melt and fluid inclusions

Anna M. Nikolenko [a,*], Anna A. Redina [a], Anna G. Doroshkevich [a,b,c], Ilya R. Prokopyev [a,d], Alexey L. Ragozin [a,d], Nikolay V. Vladykin [e]

[a] VS Sobolev Institute of Geology and Mineralogy, Siberian Branch Russian Academy of Sciences (SB RAS), pr. Akademika Koptyuga 3, 630090 Novosibirsk, Russia
[b] The Geological Institute of SB RAS, st. Sakhyanova 6a, 670047 Ulan-Ude, Russia
[c] National Research Tomsk State University, 36, Lenin ave., 634050 Tomsk, Russia
[d] Novosibirsk State University, st. Pirogova 2, 630090 Novosibirsk, Russia
[e] Vinogradov Institute of Geochemistry and Analytical Chemistry, Russian Academy of Sciences, ul. Favorskogo 1a, 664033 Irkutsk, Russia

ARTICLE INFO

Article history:
Received 21 May 2018
Accepted 24 August 2018
Available online 4 September 2018

Keywords:
Magnetite-apatite rocks
REE mineralization
Mineralogy
Geochemistry
Melt and fluid inclusion study

ABSTRACT

The concentration and redistribution of ore components from a primary melt to hydrothermal fluids are important for understanding ore formation. The Mushgai-Khudag complex is a typical example of an intrusion where hydrothermal processes are widespread and where we can observe the redistribution of ore components during hydrothermal processes. In this study, we use mineralogical, melt and fluid inclusion data to trace element characteristics of apatite from the Mushgai-Khudag complex to reconstruct the formation of the magnetite-apatite rocks and their magmatic-hydrothermal evolution and to clarify the origin of the REE mineralization. We conclude that the magnetite-apatite rocks crystallized from salt melt with a high content of phosphate and sulfate components at a temperature of approximately 830–850 °C. The origin of magnetite-apatite rocks probably can be explained by the silicate-salt immiscibility that occurred at the alkaline syenite crystallization stage. Further evolution of the salt melt to the brine of the carbonate-(fluoride)-chloride-sulfate composition was accompanied by the barite, celestite and monazite-Ce formation at the temperature of approximately 500–580 °C. The dissolution of apatite and the crystallization of gypsum, phosphosiderite and monazite-Ce pseudomorphs after apatite took place at the hydrothermal stage after a reaction with a fluid that evolved from carbonate-chloride-sulfate (at 250–350 °C) into a predominantly chloride composition (at 150–250 °C). The high activity of the sulfate component and a significant enrichment of the rocks in REE also occurred at the late hydrothermal stage.

1. Introduction

Magnetite-apatite rocks are known to host significant economic deposits of phosphorus, iron and titanium. The deposits are typically associated with intrusive complexes that consist of the following: (1) alkaline silicate rocks and carbonatites, such as the Khibiny and Kovdor in Russia, the Palabora in South Africa, and others; (2) anorthosites, such as the Nelson in Virginia; and (3) intermediate-to-felsic volcanic-subvolcanic rocks, such as Kiruna in Sweden. These types of rock are, however, not similar to the same types in the Mushgai-Khudag magnetite-apatite rocks, in which the highest apatite content reaches 80–90 wt.% (Ontoev et al., 1979). The Mushgai-Khudag magnetite-apatite rocks are hosted in alkaline syenites, which are the part of ultrabasic-basic alkaline complex. From this viewpoint, the Mushgai-Khudag magnetite-apatite rocks are unique, and they have been described rarely in previous works that discuss magmatic phosphorus deposits. In addition, the rocks have great petrological importance because they may derive from unusual phosphate-rich magma or may be produced as cumulates from alkaline silicate magmas. The Mushgai-Khudag complex (in Russian, Mushugai-Khuduk) is part of the Late Mesozoic Central Asian carbonatite province (Nikiforov and Yarmolyuk, 2004). The province includes regions of carbonatite-alkaline magmatism manifestation in West Transbaikalia (e.g., Khalyuta, Oshurkovo, Torei, Yuzhnoe and Arshan carbonatites) and in Central Tyva (Karasug and Ulatay-Choz carbonatites) of Russian Siberia, and alkaline complexes manifest in South Mongolia (Mushgai-Khudag, Khotgor and Ulugey massifs). The age of the formation of alkaline silicate rocks and associated carbonatites from the Western Transbaikalia is the middle Early Cretaceous (131–118 Ma) (Bulnaev and Posokhov, 1995; Ripp et al.,

* Corresponding author.
E-mail address: nikolenkoam@igm.nsc.ru (A.M. Nikolenko).

https://doi.org/10.1016/j.lithos.2018.08.030
0024-4937/

2009b); Central Tyva carbonatites yielded a very narrow range of ages (118–117 Ma) (Nikiforov et al., 2006; Prokopyev et al., 2016; Sal'nikova et al., 2010), whereas the ages for the South Mongolia alkaline complexes have wide variations (179–121 Ma) (Samoilov and Kovalenko, 1983). The formation of carbonatite complexes within the province has been linked with the Mesozoic-Cenozoic plume-related intraplate magmatic activity (Kovalenko et al., 2004; Kuzmin and Yarmolyuk, 2014; Yarmolyuk et al., 2004 and others). The carbonatites are associated with high-K silicate rocks such as alkaline gabbro and syenite (e.g., Doroshkevich et al., 2010; Samoilov and Kovalenko, 1983) and contain a significant Fe-F-P-(Ba)-(Sr)-REE ore mineralization (Bolonin, 2007; Doroshkevich et al., 2008, 2010; Prokopyev et al., 2016; Vladykin, 1997).

The geology, geochemistry, and petrography of the rocks and inclusions in the minerals of the Mushgai-Khudag complex have been described in numerous publications (Andreev and Khubanov, 2005; Andreeva et al., 1998; Andreeva and Kovalenko, 2003; Baatar et al., 2013; Baskina et al., 1978; Enkhbayar et al., 2016; Krmíček et al., 2010; Kynický and Samec, 2005; Ontoev et al., 1977; Samoilov and Kovalenko, 1983; Ripp et al., 2005; Vladykin, 2013), and it was found that REE mineralization is associated with carbonatites, fluorite mineralization and magnetite-apatite rocks (Andreev and Khubanov, 2005; Enkhbayar et al., 2016; Ontoev et al., 1979; Ripp et al., 2005; Rundqvist et al., 1995).

Andreeva and Kovalenko (2003) estimated the conditions for the formation of rocks of the Mushgai-Khudag complex through the study of melt inclusions and demonstrated that the rocks were formed by processes of crystallization differentiation and salt-silicate liquid immiscibility at a temperature above 1200 °C. The authors concluded that the ore-bearing magnetite-apatite rocks had been formed during an early stage of the alkaline magmatism of the Mushgai-Khudag complex, but the exact values of the homogenization temperatures for the melt inclusions were not determined. Moreover, it was proposed that the parental salt magma of the magnetite-apatite rocks was characterized by a great diversity of unusual compositions comprising high Sr, Ce, La, F and carbonate content at the weight percent levels (Andreeva, 2000; Andreeva et al., 1998; Andreeva and Kovalenko, 2003).

In this paper, we present new data on the mineral composition of the magnetite-apatite rocks and trace element data for the apatite, melt and fluid inclusion study showing the evolution of the parental magma to hydrothermal fluid solutions, and attempt to explain the specific conditions for hydrothermal alteration and the formation of the REE mineralization of the magnetite-apatite rocks in the Mushgai-Khudag complex.

2. Geological setting

The Mushgai-Khudag carbonatite-alkaline complex is located in the southern part of Mongolia in the Gobi Desert (Fig. 1). The complex is composed of nephelinites and alkali feldspar trachytes, which are crosscut by stocks and dykes of alkaline syenites, shonkinites and magnetite-apatite rocks, as well as numerous small dykes of fine-grained carbonatites (Fig. 2a) (Samoilov and Kovalenko, 1983; Vladykin, 2013). The latest fluorite mineralization is widespread in the Mushgai-Khudag area. It occurs as disseminations in host rocks and forms the nets of microveinlets as well as veins up to a few meters wide. Many zones of mineralization are brecciated and carry fragments of host rock.

Country rocks are represented by Palaeozoic sedimentary-volcanogenic facies (limestones, sandstones, argillaceous shales and basic effusive rocks) and Carboniferous granitoids. The complex is positioned within a sub-latitudinal graben belonging to a major rifting system (Samoilov and Kovalenko, 1983). Faults of the north-east and north-west directions control the position of subvolcanic intrusive bodies. There are also ring structures 0.5 to 2 km in diameter. Alkali feldspar trachyte vent facies with carbonatite veins and pyroclasts are positioned at the centre of those structures (Baskina et al., 1978).

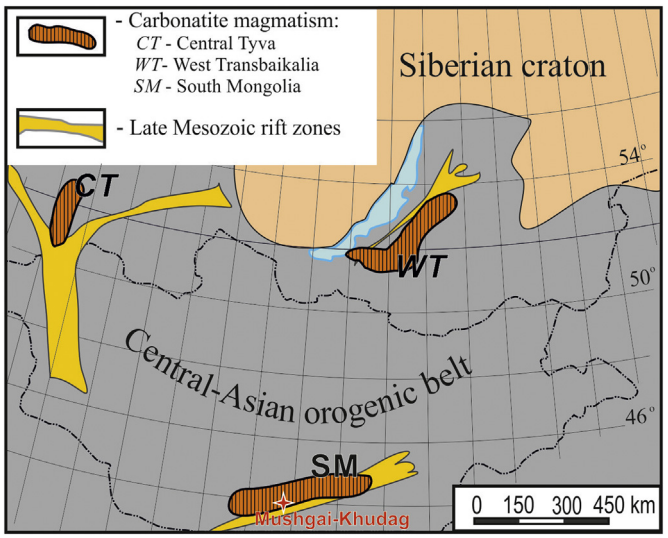

Fig. 1. Simplified map of the Late Mesozoic Central Asian carbonatite province after (Kovalenko et al., 2004; Kuzmin and Yarmolyuk, 2014), with additions by the authors.

Nephelinites form extrusive sheets up to 50 m in thickness. They are dark porphyritic rocks containing up to 20% phenocrysts. The phenocrysts are represented predominantly by phlogopite (up to 5 mm in size) and, additionally, by clinopyroxene and apatite (Fig. 3a). The fine-grained groundmass is composed of phlogopite, clinopyroxene, albite, K-feldspar, while apatite, magnetite and titanite are minor and accessory. With regards to the content of normative nepheline and albite (Le Bas, 1989), the rocks are plotted in the fields of basanite and nephelinite of the TAS diagram. Alkali feldspar trachytes form lava flows or remnants of paleovolcanos up to 10–350 m in thickness. The phenocrysts (approximately 15–20 vol.%) are represented predominantly by K-feldspar, phlogopite and apatite, minor magnetite and clinopyroxene (Fig. 3b). The normative composition of aphyric varieties comprises 48 wt.%, plagioclase, 32 wt.% orthoclase and approximately 9 wt.% hypersthene.

Shonkinite forms vein bodies up to 150 m in length. It is a grey fine- to medium-grained rock with a porphyric texture. Porphyric grains are predominantly phlogopite, clinopyroxene or K-feldspar, as well as magnetite and apatite (Fig. 3c). K-feldspar crystals often form intergrowths and are surrounded by fine-grained phlogopite rims. Apatite occurs as grey elongated prismatic crystals up to 1 cm in size. The groundmass minerals are K-feldspar, phlogopite, and magnetite. Alkaline syenites form dykes, stocks and small massifs from a few metres to 1 km wide. They are light grey or greenish-gray porphyritic rocks, the phenocrysts of which are represented by K-feldspar, minor phlogopite, clinopyroxene, magnetite and apatite. Fine- and medium-grained K-feldspar is a predominant mineral of the groundmass (Fig. 3d). The rocks are characterized by the presence of apatite-magnetite schlieren, from a few to tens of cm in size (Fig. 4a, b). The magnetite grains reach up to 4 cm in length. In schlieren, apatite fills interstitial spaces between magnetite grains. Sometimes, apatite-phlogopite rims are observed in contact with host alkaline syenites.

Carbonatites compose veins and dykes from a few cm to 10 m wide. The main minerals of carbonatites are calcite, dolomite and fluorite. The minor and accessory minerals are celestite, barite, apatite, goethite, monazite-Ce, REE fluorocarbonates (bastnaesite, parisite). Carbonatites are ubiquitously associated with fluorite mineralization. Fluorite veins and stock-like bodies are widespread and consist of fluorite-calcite, fluorite-barite, fluorite-quartz, and fluorite-celestite in mineral composition.

Apatite and magnetite-apatite rocks are exposed in two stocks 30 x 70 and 10 x 30 m in size (Fig. 2b) within an alkaline syenite field. The former stock is called Apatite Hill. Monomineral, very coarse-grained

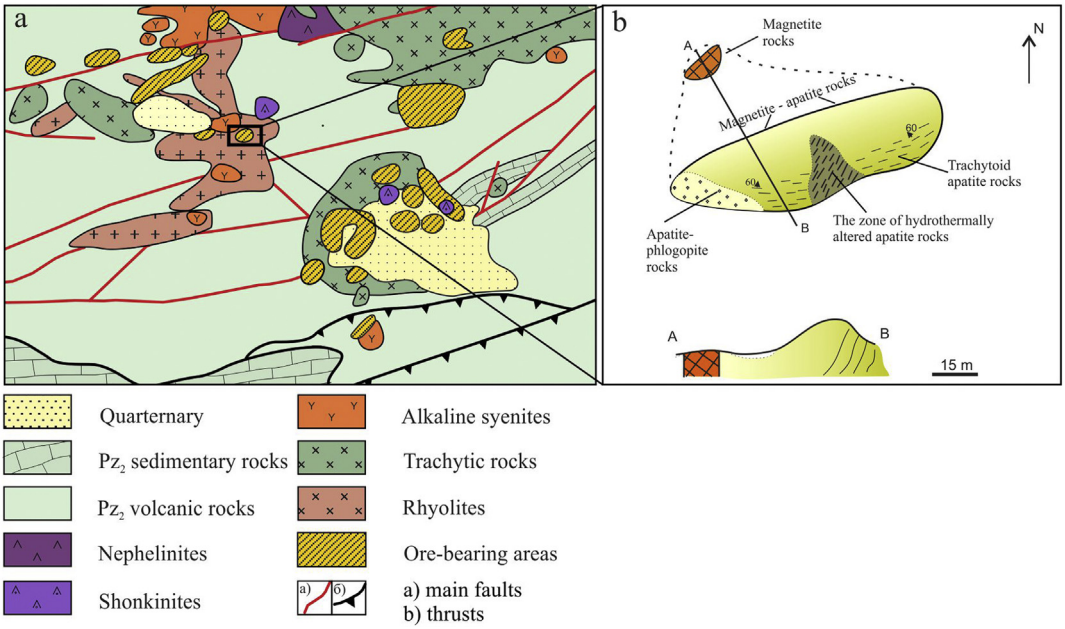

Fig. 2. Simplified geological map of the Mushgai-Khudag Complex (a) and geological scheme of the Apatite Hill (b) after (Samoilov and Kovalenko, 1983), with additions by the authors.

magnetite rocks comprise the central parts of the stock. Towards the margins, the rocks gradually change to magnetite-apatite (apatite appears in the interstices) and then apatite - phlogopite and pure apatite rocks. Apatite and phlogopite form crystals up to 10–20 cm in size. Contacts with the host alkaline syenites are not exposed. The apatite rocks near the contacts are brown or yellowish-brown and acquire a trachytic texture (Fig. 4c). There are no phlogopites in these parts of the rocks. In the southern part of the Apatite Hill, there is a 3 × 5 m zone of hydrothermally altered apatite and magnetite-apatite rocks. The rocks have a mealy appearance of whitish and greenish shades (Fig. 4d).

The available absolute K-Ar geochronological data (Samoylov and Kovalenko, 1983) for the Mushgai-Khudag rocks have wide variations

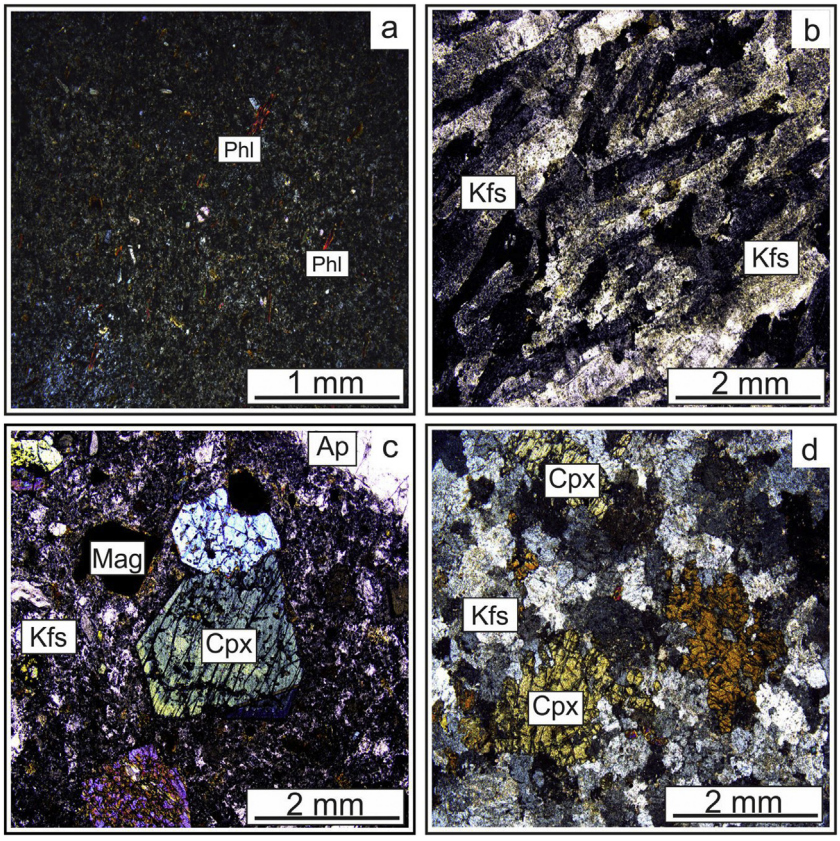

Fig. 3. Photomicrographs of typical silicate rocks of the Mushgai-Khudag complex: a) nephelinite; b) alkali feldspar trachyte; c) shonkinite; d) alkaline syenite. Abbreviations: cpx - clinopyroxene, mag - magnetite, ap – apatite, kfs – K-feldspar.

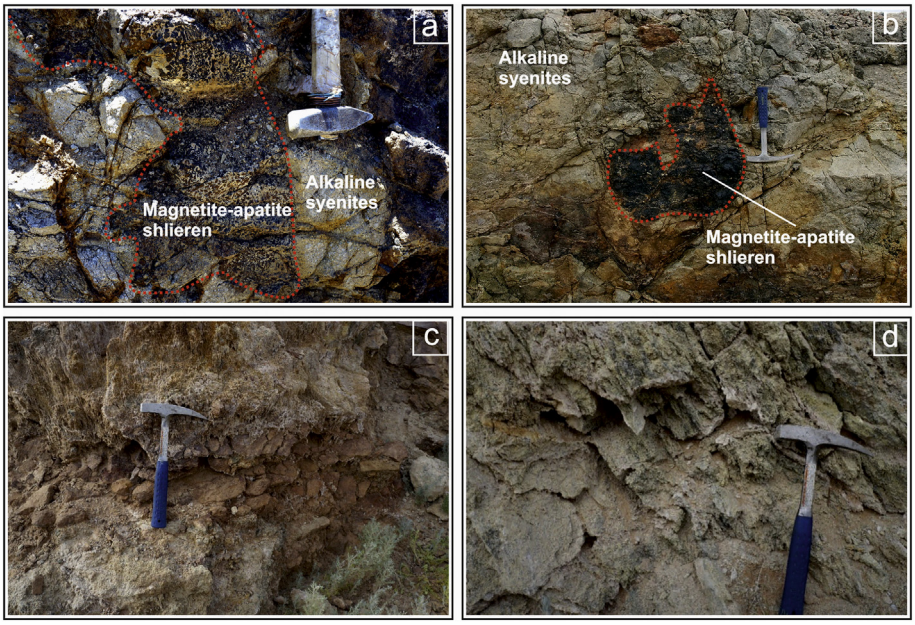

Fig. 4. Photos of the magnetite-apatite rocks from Apatite Hill: a, b – magnetite-apatite shlieren in host alkaline syenites; c – a brownish apatite rocks near the contact; d – a zone of hydrothermally altered apatite and magnetite-apatite rocks.

between 179 and 121 Ma: the ages of shonkinites range from 148 to 138 Ma; alkaline syenites - 179-140 Ma; and magnetite-apatite rocks - 138-121 Ma. However, the K-Ar method of dating is susceptible to being reset by secondary processes is not be reliable. The single Rb-Sr isochron age of alkaline syenites: 139.9 ± 5.9 Ma (Baatar et al., 2013).

3. Analytical methods

Rock textures and mineral assemblages were studied using an optical petrographic microscope and energy-dispersive spectrometry (EDS) in combination with back-scattered electron imaging (BSE) using a MIRA 3LMU SEM (TESCAN) equipped with an INCA Energy 450 XMax 80 microanalysis system (Oxford Instruments Ltd.).

Electron microprobe analyses (EMPA) with wavelength-dispersive spectrometry (WDS) were done using the JXA-8100 electron microprobe. The operating conditions were chosen to minimize devolatilization: beam diameter of 1–2 μm, accelerating voltage of 20 kV and a beam current of 15–25 nA, counting time of 5 s for Na and Fe, 10 s for F, Nb, Ti, Si, K, Ca, Nd, Zr, U, Pr, Th, Ce, Sr, Pb, La, Ba and 20 s for Y. Data reduction was performed using a PAP routine (Pichou and Pichoir, 1984). The received BSE-images were used to select appropriate points for quantitative electron microprobe analyses. The following standards were used for quantification of the elements: diopside (Si-Kα, Ca-Kα), albite (Na-Kα), fluorphlogopite (F-Kα, K-Kα), synthetic $LiNbO_3$-REE (Nb-Lα), TiO_2 (Ti-Kα), Fe_2O_3 (Fe-Kα), $NdPO_4$ (Nd-Lα), zircon (Zr-Lα), $PrPO_4$ (Pr-Lα), UPO_4 (U-Mα), YPO_4 (Y-Lα), ThO_2 (Th-Mα), $CePO_4$ (Ce- Lβ), $Pb_2P_2O_7$ (Pb-Mα), $LaPO_4$ (La-Lα), Sr-glass (Sr-Lα), Ba-glass (Ba-Lα). Relative standard deviation was less 2%.

Raman spectra were collected using a Horiba Jobin Yvon LabRAM HR800 Raman microspectrometer equipped with a 532-nm Nd: YAG laser and an Olympus BX41 microscope. The RRUFF project database and CrystalSleuth application (http://rruff.info/) were used for mineral identification. Heating and freezing experiments for fluid inclusion study were carried out using heat chamber TC-1500, with an inert atmosphere of purified argon, and a Linkam THMSG-600 stage for determination of melting and homogenization temperatures of inclusions.

All the above listed analyses were carried out at the Analytical Center for multi-elemental and isotope research in the Siberian Branch of the Russian Academy of Science (Novosibirsk, Russia).

Concentrations of trace elements in apatite were determined at the Novosibirsk State University by LA-ICP-MS analyses using the quadrupole-based inductively coupled plasma mass spectrometer (XSeries 2, Thermo Scientific, Germany) coupled to a laser ablation system (NWR 213, New Wave Research, USA). Analyses were performed for a large group of elements including Sc, V, Mn, Sr, Y, Zr, Nb, Ba, Hf, Ta, Pb, Th, U and all the lanthanides from La to Lu. NIST 612 glass was used as an external standard for calculations of element concentrations in apatite. Calcium contents in apatite determined by microprobe analysis were in the range of 48–52 wt.% CaO and they were used as an internal standard in calculations.

The oxygen isotope compositions in apatite and phlogopite were determined at the Geological Institute SB RAS (Ulan-Ude, Russia) using Finigan MAT 253 sensitive mass spectrometers. Oxygen isotope analyses were carried out using the laser-fluorination method developed by Sharp (1990). Samples were heated up with a 100 W CO_2 laser in a BrF_5 atmosphere. The $\delta^{18}O$ values obtained in this study were checked against international reference materials NBS-28 quartz (9.65‰; n = 11) and NBS-30 biotite (5.11‰; n = 21). The garnet standard UWG-2 (5.88‰) was analyzed during each run to ensure accuracy. On the basis of these data and the reproducibility of duplicate measurements, the $\delta^{18}O$ values of samples are accurate to within 0.2‰.

4. Petrography and mineral chemistry of magnetite-apatite rocks

Magnetite-apatite rocks are brown, greenish-grey, dark grey with massive or trachytoidal in texture. Some of them show variable degrees of hydrothermal alteration and, in the following description, we will use the term “unaltered rocks” for unaltered and slightly altered magnetite-apatite rocks, and the term “altered rocks” for magnetite-apatite rocks with strong and clear signs of hydrothermal alteration. The main minerals of the magmatic association are apatite, magnetite, ilmenite and phlogopite. Minerals of the hydrothermal stage are goethite, phosphosiderite, monazite-Ce, celestite, rutile, quartz, fluellite, fluorite, barite, gypsum and pyrite. Modal proportions of apatite and magnetite, which together constitute together approximately 90% of the rock, vary considerably. Apatite in unaltered rocks forms idiomorphic crystals range in size from a few mm to 10–15 cm in pegmatoid areas. Magnetite forms isometric grains from several mm to 10 cm in size. Magnetite contains ilmenite lamellae oriented in the [111] direction. Phlogopite is

observed as flakes up to 20 cm in size, usually in association with apatite. Gypsum is found as randomly oriented plates in apatite (Fig. 5a, b). Apatite hosts rare inclusions of monazite-Ce and, in the case of intensive hydrothermal reworking, the monazite-Ce forms a net of very fine microveins along the cracks and rims around the apatite grains (Fig. 5c). In the areas of the strongest hydrothermal alteration, monazite-Ce and phosphosiderite replace apatite by forming partial or complete pseudomorphs (Fig. 5d, e). Celestite is represented by rare grains in association with phosphosiderite and monazite-Ce.

Apatite corresponds to fluorapatite (F up to 1.6 wt.%). Representative compositions of apatites are given in Table 1. In the unaltered rocks, the mineral contains SiO_2 (up to 2.1 wt.%), SO_3 (up to 1.8 wt.%) and Na_2O (up to 0.8 wt.%). The content of light rare earth elements (LREE) in the unaltered apatite is up to 4.5 wt.%. The average ratios of REE in the mineral composition are Ce/La = 1.6, Ce/Nd = 2.6 and La/Nd = 2. The mineral in BSE has an internal spot-zonal structure due to variations in the composition of admixture components, where the dark zones contain a lower amount of LREE than do the light zones (Fig. 5 f). This finding is consistent with experimental studies (Harlov et al., 2003), which confirmed that the internal redistribution of REE may be due to metasomatic processes. According to Ripp et al. (2005), such variations are related to the recrystallization of the Mushgai-Khudag apatite crystals. Apatite from altered rocks has a higher LREE and silica content than that of the apatite from unaltered rocks (Fig. 6). The content of SiO_2 increases up to 6.6 wt.% in the altered rocks, and the sum of REE_2O_3 reaches 15.0 wt.%. The average ratios of REE for the apatite from altered rocks are Ce/La = 1.2, Ce/Nd = 3.2, and La/Nd = 3.6. Similar changes in the Ce/Nd ratio have been found to result from hydrothermal processes (Fleischer, 1978), including those described in several carbonatitic occurrences (Doroshkevich et al., 2008; Zaitsev et al., 1998). The change may manifest in the transition from carbonatite magma to a "carbothermal" fluid (Mitchell, 2005).

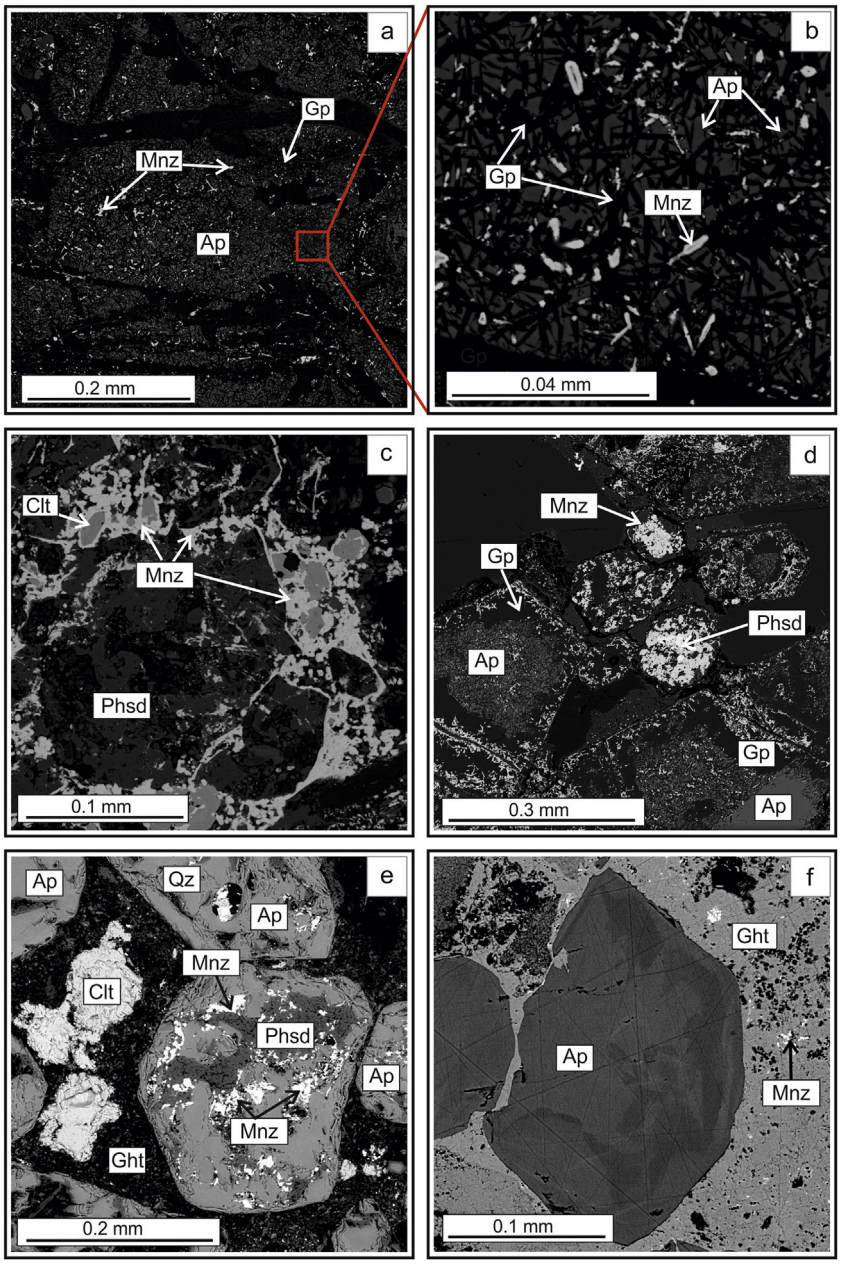

Fig. 5. The BSE images of magnetite-apatite rocks from the Mushgai-Khudag complex: a, b - differently oriented plates of gypsum in apatite; c - a net of the finest microveinlets of monazite-Ce along the cracks and in the rims of apatite completely replaced by phosphosiderite; d, e - partial or complete pseudomorphs of phosphosiderite replacing apatite; e - spot-zonal structure of apatite.

Table 1
Representative analyses of apatites from magnetite-apatite rocks.

	Unaltered rocks			Altered rocks										
	1	2	3	1	2	3	4	5	6	7	8	9	10	11
CaO	50.46	52.28	50.95	50.32	50.02	50.47	50.91	49.58	49.63	49.87	47.78	46.98	45.58	43.85
Na_2O	0.49	0.58	0.77	0.66	0.38	bdl	bdl	0.34	0.23	bdl	0.28	bdl	0.34	0.23
SrO	0.45	0.54	0.46	0.52	0.49	0.48	0.47	0.45	0.50	0.55	0.56	0.45	0.53	0.49
Ce_2O_3	2.12	1.70	2.60	3.69	3.30	3.31	3.58	3.54	3.82	4.08	4.94	6.36	6.49	7.70
La_2O_3	1.09	bdl	1.17	1.47	1.41	1.65	2.25	2.18	2.49	2.25	3.64	4.00	3.70	4.89
Pr_2O_3	bdl	bdl	bdl	bdl	bdl	bdl	bdl	bdl	bdl	bdl	bdl	bdl	0.56	0.55
Nd_2O_3	0.82	0.45	0.73	bdl	0.84	0.80	0.75	0.99	1.01	1.18	1.45	1.40	1.50	1.75
REE_2O_3	*4.03*	*2.15*	*4.50*	*5.16*	*5.55*	*5.76*	*6.58*	*6.71*	*7.32*	*7.51*	*10.03*	*11.76*	*12.25*	*14.89*
P_2O_5	39.82	39.62	37.85	35.38	36.43	33.18	30.77	33.61	31.83	30.89	30.50	30.09	30.66	30.7
SiO_2	1.60	1.63	2.10	3.68	3.27	4.73	5.52	4.71	5.48	5.67	5.93	6.23	6.38	6.57
SO_3	0.80	0.70	1.80	2.82	1.85	3.30	3.95	3.12	3.35	3.77	3.25	2.30	2.40	1.67
F	3.65	3.65	3.29	3.63	3.76	3.51	3.21	3.13	3.35	2.57	2.87	3.03	3.76	3.23
Total	101.30	101.15	101.72	102.17	101.75	101.43	101.41	101.65	101.69	100.83	101.20	100.84	101.90	101.63
$-O=F_2$	1.53	1.53	1.38	1.52	1.57	1.47	1.35	1.31	1.41	1.08	1.21	1.27	1.56	1.36
Total	99.77	99.62	100.34	100.65	100.18	99.96	100.06	100.34	100.28	99.75	99.99	99.57	100.34	100.27
Ca *apfu*	4.412	4.650	4.453	4.408	4.392	4.413	4.450	4.380	4.383	4.389	4.272	4.203	4.171	4.086
Na	0.078	0.094	0.124	0.106	0.061	-	-	0.054	0.038	-	0.048	-	0.054	0.038
Sr	0.022	0.026	0.023	0.025	0.024	0.023	0.023	0.022	0.024	0.026	0.026	0.022	0.026	0.024
Ce	0.064	0.052	0.079	0.112	0.101	0.102	0.112	0.107	0.118	0.128	0.157	0.206	0.205	0.245
La	0.033	-	0.036	0.045	0.043	0.051	0.071	0.067	0.077	0.071	0.116	0.130	0.119	0.157
Pr	-	-	-	-	-	-	-	-	-	-	-	-	0.018	0.017
Nd	0.024	0.014	0.022	-	0.025	0.024	0.023	0.029	0.031	0.036	0.045	0.044	0.046	0.054
P	2.777	2.796	2.670	2.488	2.579	2.355	2.226	2.357	2.275	2.237	2.235	2.250	2.242	2.259
Si	0.132	0.136	0.175	0.306	0.274	0.396	0.472	0.390	0.462	0.485	0.513	0.550	0.551	0.571
S	0.049	0.044	0.112	0.176	0.116	0.207	0.253	0.194	0.212	0.242	0.211	0.152	0.155	0.109
OH	0.049	0.038	0.133	0.046	0.006	0.069	0.132	0.180	0.105	0.305	0.214	0.154	0.006	0.112
F	0.951	0.962	0.867	0.954	0.994	0.931	0.868	0.820	0.895	0.695	0.786	0.846	0.994	0.888

Note: b.d.l. - below detection limit; apfu – atom per formula units are based on 12 oxygens.

Apatite compositions from unaltered magnetite-apatite rocks are characterized by the strong enrichments in LREE with La/Yb ratio is 145–150 (Fig. 7, Table 2). The chondrite-normalized REE patterns are steep and relatively smooth, and show a slightly negative Eu anomaly with Eu*/Eu from 0.49 to 0.63. In contrast, apatite from hydrothermally altered magnetite-apatite rocks shows strong increase in LREE and the REE chondrite-normalized patterns show no negative Eu anomaly (Fig. 7, Table 2). In comparison with apatite from magnetite-apatite rocks, apatite from shonkinites shows lower REE levels and no Eu anomaly (Nikolenko and Doroshkevich, 2017). The chondrite-normalized REE plots of apatite from alkaline syenite are generally steep with a weak negative Eu anomaly, with Eu*/Eu from 0.37 to 0.53.

Magnetite is characterized by the presence of TiO_2 (up to 0.6 wt.%) and Al_2O_3 (up to 3.0 wt.%) (Table 3). The feature of composition of ilmenite lamellae in magnetite is the presence of V_2O_3 admixture (Table 3). Sometimes, rutile (or anatase?) replaces ilmenite; the mineral contains Nb_2O_3 and ZrO (Table 3). Magnetite is often replaced by haematite along the edges and along the cracks. The haematite contains TiO_2 (up to 0.6 wt.%) (Table 3). In the areas of the most intensive hydrothermal reworking magnetite is almost completely replaced by goethite.

Phlogopite is characterized by a high amount of TiO_2 (up to 3.3 wt.%) and F (up to 2.1 wt.%). The characteristic feature of the mineral composition is the presence of Na_2O (up to 0.9 wt.%) (Table 4). The average composition of phlogopite corresponds to the formula: $(K_{1.69}Na_{0.17})_{1.9}(Mg_{4.42}Fe_{1.10}Ti_{0.32}Mn_{0.03})_{5.9}(Si_{5.92}Al_{2.03})_{7.9}O_{20}(F_{1.95}OH_{2.05})_{4.0}$. The phlogopite composition is similar to that of micas from the Late Mesozoic carbonatite complexes of the West Transbaikalia (Ripp et al., 2009a) (Fig. 8).

Monazite-Ce is unique in containing sulfur (up to 10 wt.% SO_3), and it is also enriched in SrO and CaO (up to 6.5 wt.% and 5.5 wt.%, respectively) (Table 5). The mechanism of substitution was inferred by Kukharenko et al. (1965) for "sulfate-monazite" from Vuoriyarvi and by Chakhmouradian and Mitchell (1999) for monazite from the Internatsronal'naya kimberlite pipe in Yakutia. Such scheme also was proposed for monazite-Ce from the Mushgai-Khudag magnetite-apatite rocks (Enkhbayar et al., 2016): $Ce^{3+} + P^{5+} \leftrightarrow Ca^{2+}$ (Sr^{2+}) + S^{6+}.

The accessory minerals of hydrothermal association are barite, celestite, fluorite, phosphosiderite, and fluellite. The presence of SrO up to 2.0 wt.% is typical for barite. Celestite is characterized by the presence of BaO up to 5.0 wt.%. Fluellite and phosphosiderite were first identified in the the Mushgai-Khudag complex by the authors. The Raman spectrum of phosphosiderite has typical peaks at 285, 480, and 985 cm^{-1} (Fig. 9). The phosphosiderite contains SO_3 up to 0.8 wt.%, SiO_2 up to 3.5 wt.%, Al_2O_3 up to 6.4 wt.%.

5. Isotope geochemistry

Oxygen isotope composition of apatite from unaltered rocks is characterized by the $\delta^{18}O$ values from 5.1 ‰ to 5.6 ‰. Phlogopite has the $\delta^{18}O$ value of 7.3 ‰. The values are similar to those that are typical for mantle-derived igneous rocks (Hoefs, 2015), including carbonatite (Demény et al., 2010; Doroshkevich et al., 2010, 2016; Tichomirowa et al., 2006). The $\delta^{18}O$ values of the minerals are within the same range as those observed in the silicates and apatite (5.5–7.2 ‰) from the West Transbaikalia alkaline silicate rocks and carbonatites (Demény et al., 2010; Doroshkevich and Ripp, 2009; Nikiforov et al., 1998). In addition, apatite from iron oxide-apatite deposits of Kiruna type show stronger $\delta^{18}O$ variation, from 5.5 to 12.2 ‰ (Ripp et al., 2017; Yu et al., 2015).

The altered apatite shows heavier $\delta^{18}O_{SMOW}$ (6.0 to 7.5 ‰) than that of the unaltered mineral. The $\delta^{18}O$ change observed for altered apatite may be interpreted as the result of post-magmatic isotope exchange with hydrothermal fluids, which can be post-magmatic aqueous fluids or low-temperature crustal water, as well as a mixture of these. Fluid inclusions (see section 6 below) in altered apatite only testify that it was low-temperature (250–150 °C) aqueous fluid.

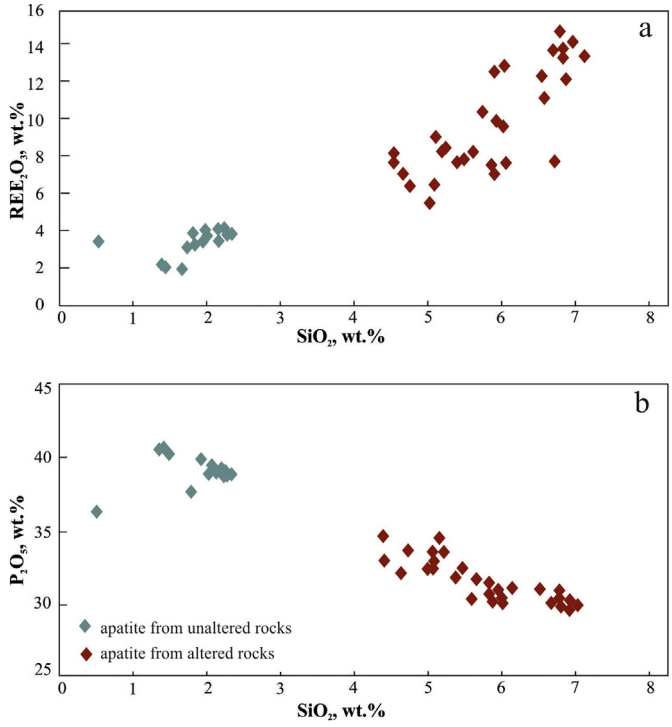

Fig. 6. Compositional variations of P_2O_5/SiO_2 and REE_2O_3/SiO_2 (wt.%) ratios of apatites from unaltered and altered magnetite-apatite rocks from the Mushgai-Khudag complex.

6. Melt and fluid inclusion study

By optical investigations, we have identified three types of inclusions in the apatite of the magnetite-apatite rocks: melt inclusions, brine-melt and crystal-fluid inclusions of different generations (Fig. 10).

Melt inclusions were found in central parts of the apatite crystals (Fig. 10a). There are isolated single inclusions or groups of up to 3 inclusions. The inclusions have oval shapes and are 7–30 μm in size. The inclusions contain micro-granular aggregates of silicate-salt composition and the gas phase (1–3 vol. %). The homogenization temperature for the melt inclusions in the apatite crystals varies in the interval from 740 to 850 °C, and for the small melt inclusions, the homogenization temperatures mostly fall within 830–850 °C (Fig. 11a). During heating experiments at temperatures above 500 °C, the salt phases of the inclusions start melting, and the segregation of the fluid phase begins; at the temperatures of more than 650 °C, the melting of the last saline component occurs and we observe two separate melt and fluid phases; and with further heating, the fluid phase volume decreases and the inclusions homogenize into the liquid phase in the interval of 740–850 °C. When the sample is cooled, the inclusions are restored to their original forms. According to the Raman data, the melt inclusions contain a mixture of silicate and salt phases, predominantly of a phosphate, carbonate and sulfate composition (Fig. 11b). SEM investigations of opened melt inclusions in the apatite crystals show the presence of the silicate phase of composition close to the Na amphibole. The opened inclusions also revealed small daughter phases of anhydrite (Fig. 11c). Unfortunately, we could not identify the remaining salt phases (carbonate and phosphate, and probably chloride) in the composition of the melt inclusions on the basis of their small size and instability after the opening of the inclusions. We believe that the salt mineral assemblage is close to that in brine-melt inclusions. Another type of inclusion is a highly concentrated (~ 89–97 wt.% of the solute) brine-melt fluid of the silicate–carbonate-(fluoride)-chloride-sulfate composition (Fig. 10b–f). The inclusions are found in groups and located along the growth zones of the apatite crystals. The inclusions are elongated and have negative crystal shapes. Their size ranges from 10 to 70 μm and the inclusions could be classified as pseudo-secondary. The salt-fluid inclusions contain up to 10 different crystal phases and a CO_2 liquid phase. According to the Raman data and SEM analyses of opened brine-melt inclusions, there are daughter phases of anhydrite, celestite (Ba-bearing), sodic amphibole (?), monazite-Ce, haematite, fluorite, apatite and Na/K chloride (Fig. 12). The homogenization temperatures vary broadly for the brine-melt inclusions and, in our view, this implies a heterogeneous trapping of xenogeneic solid phases; for example, fluorite and apatite (Figs. 10f and 12a). Andreeva et al. (1998) reported similar observations. Therefore, we measured the homogenization temperature only for small, highly concentrated crystal-fluid inclusions located within the same apatite growth zone and containing only one or two daughter phases (usually of sulfate composition). The measured values fell into the interval of 500–580 °C.

Secondary fluid inclusions in the apatite crystals of unaltered and predominantly altered rocks are represented by two types: crystal-fluid and gas–liquid fluid inclusions (Fig. 10g-i). Secondary fluid inclusions have elongated, negative crystal or irregular forms; they are 4–10 μm in size, and the fluids fill cracks and planes. The crystal-fluid inclusions in the apatite crystals of the unaltered rocks contain a CO_2 gas phase (1–3 vol.%), one to ten daughter crystal phases including halite/sylvite (rare), celestite, anhydrite, haematite and monazite occupying 3–10 vol.% in total, and a liquid aqueous solution (Fig. 10g). The homogenization temperature ranges from 250 to 350 °C. Our previous fluid inclusion investigations revealed the presence of crystal-fluid inclusions in the hydrothermal fluorites of the Mushgai-Khudag complex, containing CO_2 gas (10–15 vol.%), aqueous solution, cubic crystals of NaCl and 1–2 small crystals (~1–2 vol.%) of siderite, haematite, and phosphosiderite (Redina and Prokopyev, 2017). Fluid inclusions in the fluorite were homogenized at 360–420 °C and have the salinity of 10–20 wt.% NaCl-eq. The homogenization temperature of the secondary gas–liquid fluid inclusions of the altered magnetite-apatite rocks (recrystallized apatite grains) ranges from 250 to 150 °C (Fig. 10h–i). The crystal phases are represented by the isotropic chlorides of Na/K, with a salt concentration of 9.2–6.4 wt.% NaCl-eq., according to the freezing data. The fluid phase of the inclusions contains a mixture of CO_2 gas with water. The altered apatite grains also contain planes with substantial gaseous fluids, which probably resulted from the boiling processes.

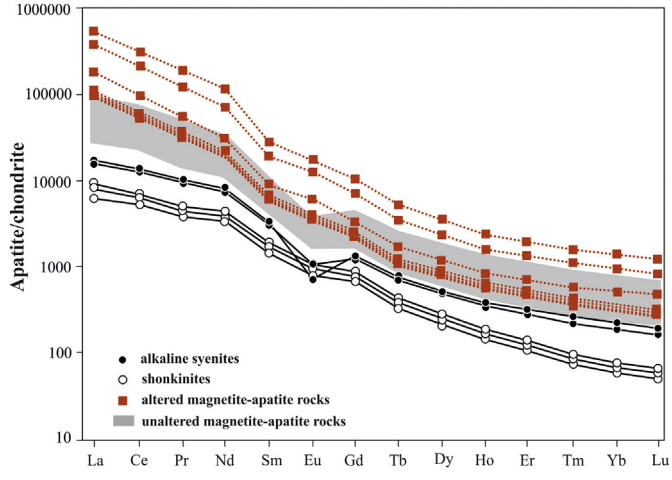

Fig. 7. Chondrite-normalized distribution of REE in apatites from shonkinites and alkaline syenites (after Nikolenko and Doroshkevich, 2017), unaltered and altered magnetite-apatite rocks. Normalizing values for chondrite are from Sun and McDonough (1989).

Table 2
Trace elements concentrations (ppm) in apatites from magnetite-apatite rocks.

	Unaltered rocks					Altered rocks						
	1	2	3	4	5	1	2	3	4	5	6	7
Sc	0.18	0.68	1.24	0.59	0.76	2.34	2.03	1.62	1.90	14.45	56.60	75.87
V	53.29	49.06	46.82	33.56	88.76	148.41	182.06	162.90	161.67	208.36	231.37	556.97
Mn	646.95	650.41	655.39	605.10	772.55	490.36	545.38	409.12	418.65	910.22	766.79	1128.82
Sr	3803.50	3973.21	4848.96	3860.40	1375.14	25903.25	23042.21	4210.23	4208.22	6962.48	19238.97	78035.64
Y	948.58	1031.48	1004.92	962.98	1582.45	980.87	826.38	899.63	889.10	1564.03	2895.14	4386.40
Zr	11.54	9.18	11.34	6.00	36.09	36.11	36.24	34.44	33.07	427.74	826.36	1270.33
Nb	0.12	0.13	0.19	0.07	0.58	1.14	0.91	1.50	1.53	1.51	2.00	3.90
Ba	10.05	36.77	36.96	8.87	1.79	616.66	599.48	31.44	28.79	60.98	72.27	1862.46
La	8540.43	8792.90	8494.36	7651.42	14650.21	19977.58	18094.05	17533.82	18925.40	39033.18	83536.62	116424.58
Ce	18859.56	19604.78	20116.95	17577.06	32731.55	32670.60	31564.60	29094.17	31643.54	58141.08	119753.36	175814.62
Pr	1857.55	1968.40	2009.92	1781.40	3394.26	2873.27	2685.27	2484.69	2740.21	4903.06	10828.45	15794.82
Nd	6933.08	6972.03	6648.80	6361.89	11238.11	8733.16	8042.77	7960.58	8426.57	13247.08	31986.62	48603.83
Sm	797.71	841.41	789.26	764.88	1253.97	847.98	743.69	764.49	776.41	1241.21	2610.40	3897.09
Eu	122.25	123.72	120.96	109.36	147.07	189.76	173.69	174.20	175.32	333.07	668.85	921.04
Gd	437.90	451.51	431.37	423.72	664.71	440.31	363.75	392.08	422.34	638.63	1294.66	1929.44
Tb	43.14	44.22	41.88	41.25	63.86	39.08	33.17	35.67	36.81	57.92	114.66	174.41
Dy	204.20	216.11	208.16	203.98	308.75	183.46	155.01	163.80	164.73	271.26	532.28	818.80
Ho	33.90	34.32	33.40	32.43	50.29	29.70	25.12	26.89	25.97	43.69	85.08	128.85
Er	80.15	84.23	80.19	78.85	119.58	69.78	59.40	64.53	62.61	107.67	206.18	315.82
Tm	9.90	10.31	9.50	9.46	15.13	8.66	6.72	8.13	7.98	13.23	25.48	38.69
Yb	59.46	59.61	56.75	53.36	88.40	52.60	41.51	48.02	46.09	80.70	152.54	228.28
Lu	7.41	8.07	7.51	7.22	11.58	6.23	5.34	6.16	6.08	10.90	20.00	30.15
Hf	0.11	0.11	0.29	0.11	0.34	0.14	0.20	0.19	0.25	2.93	6.52	10.33
Ta	0.01	0.01	0.03	0.00	0.01	0.05	0.06	0.07	0.06	0.03	0.06	0.06
Pb	44.15	39.55	47.54	36.50	50.09	65.83	60.29	42.79	33.75	133.71	314.63	816.51
Th	646.98	787.90	744.23	683.90	1557.74	227.55	172.74	190.53	158.37	174.13	210.26	778.48
U	37.54	38.18	42.38	33.19	90.82	139.36	117.31	87.81	95.45	242.04	552.54	1010.49
Eu/Eu*	0.63	0.61	0.63	0.59	0.49	0.95	1.02	0.97	0.94	1.14	1.11	1.03

Note: Eu/Eu* is calculated as $Eu_{Cn}/sqrt(Sm_{Cn}*Gd_{Cn})$, where the subscript Cn denotes C1 chondrite value normalized.

7. Discussion

7.1. The classification of the magnetite-apatite rocks

Apatite-magnetite assemblage occurs in association with various types of rocks, including Kiruna-type iron deposits, phoscorites, nelsonites, the alkaline gabbro-syenite series and others. Although several studies have been conducted on the Mushgai-Khudag magnetite-apatite rocks, the origin and nature of the rocks remain controversial.

Krmíček et al. (2010) interpreted the Mushgai-Khudag apatite-magnetite rocks as nelsonites. In addition, the magnetite-apatite-calcite rocks of Ulugei Khid massif of the Mesozoic alkaline complexes in South Mongolia also have been attributed to nelsonites (Kynicky and Chakhmouradian, 2011). According to the official classification of igneous rock (Le Maitre et al., 2002), nelsonite is a granular dyke rock consisting essentially of ilmenite and apatite with or without rutile. Nelsonites are defined by high concentrations of Ti and are usually associated with anorthosites (Charlier et al., 2008; Duchesne and Liégeois, 2015; Force, 1991 and others). In our opinion, the identification of the Mushgai-Khudag magnetite-apatite rocks as nelsonites is incorrect because it is inconsistent with the geological and mineralogical data, especially in relation to the low Ti content at Mushgai-Khudag.

The Kiruna-type rocks occur in many parts of the world, e.g., Bafq (Iran), within the Chilean Iron Belt, Great Bear (Canada), and Kirunavaara (Sweden) (Bookstrom, 1995; Daliran, 2002; Hildebrand, 1986; Hou et al., 2011; Nystroem and Henriquez, 1994). The rocks are associated with calc-alkaline volcanic (e.g., rhyolite, dacite) or sub-volcanic rocks (e.g., Frietsch and Perdahl, 1995). The rocks contain low-Ti magnetite and varying concentrations of fluorapatite, actinolite, and sulfide. The Kiruna-type apatites have weak LREE/HREE fractionation, negative Eu anomaly, and REE concentrations up to 2000–7000 ppm (Frietsch and Perdahl, 1995).

The low Ti concentration of the Mushgai-Khudag magnetites is consistent with that of Kiruna-type rocks. In addition, the Mushgai-Khudag apatites display negative Eu anomalies, but the anomalies are less pronounced than those of the Kiruna-type mineral. We concluded (see

Table 3
Representative analyses of magnetites, ilmenities, rutiles, haematites and goethites from magnetite-apatite rocks.

Mineral	Magnetite					Ilmenite			Rutile				Goethite				Haematite		
	1	2	3	4	5	1	2	3	1	2	3	4	1	2	3	4	1	2	3
FeO	31.96	32.37	32.05	30.68	31.05	35.85	36.97	39.28	4.73	1.83	0.81	0.42	85.9	88.6	86.26	86.35			
Fe_2O_3*	64.75	64.65	67.79	68.12	67.58												91.97	90.22	90.54
MgO				0.66				2.12									0.66		
MnO				0.44	0.63	0.77	0.65	4.61						0.32			0.44		
TiO_2	0.43	0.63	0.42	0.47	0.58	58.28	56.28	52.48	95.66	97.95	95.20	96.73	1.95	0.27	0.35	1.05	0.47	0.43	0.63
Al_2O_3	2.91	3.04	1.13	0.98	0.34	0.26	0.34			0.49			0.72	0.43	0.47	0.81	0.98	2.91	3.04
V_2O_3				0.25			0.57	bdl							0.47		0.25		
CaO												0.20							
SiO_2						bdl	bdl						0.56	0.34	1.28	0.36			
Nb_2O_5											1.53	1.29							
ZrO											1.82								
P_2O_5						0.27	0.37												
Total	100.05	100.69	101.39	101.60	100.18	95.45	95.18	101.59	100.68	101.27	99.36	98.64	89.13	89.97	88.84	88.58	94.77	93.57	94.22

* Fe_2O_3 was calculated by stoichiometry.

Table 4
Representative chemical composition of micas from magnetite-apatite rocks.

	1	3	4	5	6	8	10	13	14
SiO_2	40.75	41.16	41.8	41.16	41.23	41.33	41.1	40.28	41.72
TiO_2	3.34	3.42	2.85	2.74	2.95	2.8	2.92	3.2	2.82
$Al2O_3$	11.51	11.56	10.28	11.83	11.36	11.66	11.94	11.39	12.04
FeO	9.44	9.43	8.71	7.85	7.77	7.77	9.16	10.19	7.62
MnO	0.27	0.31	0.25	bdl	0.17	0.28	0.23	0.31	0.26
MgO	20.53	21.23	20.96	21.57	21.94	21.71	20.6	20.12	22.24
Na_2O	0.75	0.67	0.28	0.74	0.86	0.69	0.61	0.67	0.85
K_2O	9.3	9.23	9.61	8.9	8.81	8.99	9.2	8.87	9.02
F	4.27	4.30	4.63	4.25	4.78	4.11	4.27	3.93	5.11
Sum	100.16	101.31	99.37	99.04	99.87	99.34	100.03	98.96	101.68
$O=F_2$	1.79	1.81	1.94	1.79	2.01	1.73	1.79	1.65	2.15
Total	97.68	98.82	96.68	96.58	97.10	96.96	97.55	96.68	98.72
Si	5.89	5.87	6.08	5.94	5.94	5.94	5.92	5.88	5.91
Al iv	1.96	1.94	1.76	2.01	1.93	1.98	2.03	1.96	2.01
Ti	0.36	0.37	0.31	0.30	0.32	0.30	0.32	0.35	0.30
Fe	1.14	1.12	1.06	0.95	0.94	0.93	1.10	1.24	0.90
Mn	0.03	0.04	0.03	0.00	0.02	0.03	0.03	0.04	0.03
Mg	4.42	4.51	4.55	4.64	4.71	4.65	4.42	4.38	4.70
Na	0.21	0.19	0.08	0.21	0.24	0.19	0.17	0.19	0.23
K	1.71	1.68	1.78	1.64	1.62	1.65	1.69	1.65	1.63
OH*	2.05	2.06	1.87	2.06	1.82	2.13	2.05	2.18	1.71
F	1.95	1.94	2.13	1.94	2.18	1.87	1.95	1.82	2.29
Total	19.73	19.72	19.66	19.68	19.71	19.69	19.68	19.70	19.72

discussion below, in Section 7.3) that the negative Eu anomaly in apatite from the alkaline syenites and apatite-magnetite rocks appears because the rocks are the product of magmatic fractional crystallization of the parental alkaline silicate P-rich melt. This coclusion is not surprisingl as apatite is a sensitive recorder of magmatic evolutions, and Eu anomalies in apatites are typical for more fractionated rocks: syenites, granite pegmatites, granites (Belousova et al., 2002). In addition, the apatite-magnetite rocks of Apatite Hill stocks are hosted in alkaline syenites, and the latter commonly contain apatite-magnetite schlieren that testifies to their genetic relationship. These observations are not consistent with the typical association of Kiruna-type rocks with calc-alkaline silicic rocks. Moreover, the REE and Sr concentrations of the Mushgai-Khudag apatites and the degree of LREE enrichment (Fig. 13) are higher than those of Kiruna-type apatites, and the Mushgai-Khudag mineral association of magnetite, apatite and phlogopite is not similar to that of the Kiruna-type mineral assemblage.

Finally, the Mushgai-Khudag apatite-magnetite rocks may belong to phoscorites. According to the International Union of Geological Sciences (IUGS) classification of igneous rocks (Le Maitre et al., 2002), phoscorites are plutonic rocks that are predominantly composed of forsterite magnetite and apatite. Such rocks are olivine-free but are

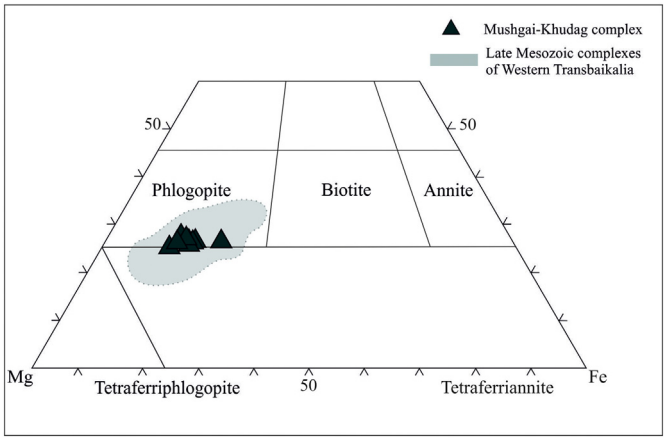

Fig. 8. Mica composition (a.p.f.u.) from the magnetite-apatite rocks of the Mushgai-Khudag complex and from carbonatite rocks of the Late Mesozoic complexes of Western Transbaikalia after Ripp et al. (2009a).

clinopyroxene- or phlogopite-bearing varieties (Krasnova et al., 2004). Phoscorites commonly reside in nephelinite-carbonatite complexes. For example, the rocks have been found in many carbonatite complexes of the Kola alkaline province, e.g., Kovdor, Seblyavr, Sokli, Turiy Mys and Vuoriyarvi (Dunworth and Bell, 2001; Krasnova et al., 2004; Kukharenko et al., 1965; Wall and Zaitsev, 2004; Zaitsev and Bell, 1995); Guli, Essei and Magan in the Maymeicha-Kotui Province (Egorov, 1992; Kogarko et al., 1991), in the Phalaborwa Complex in South Africa (Eriksson, 1989; Harmer, 2000; Russell, 1954), in Araxa, Brazil (Gittins, 1966; Issa Filho et al., 1984) and in others. Phoscorites usually contain economic apatite, Nb, Zr and REE mineralization.

There are some differences between the Mushgai-Khudag apatite-magnetite rocks and the phoscorites from the typical nephelinite-carbonatite complexes, such as the negative Eu anomaly in apatite and the absence of Nb and Zr mineralization. The differences can be explained by (1) the source characteristic for the Mushgai-Khudag primary melts that was depleted in HFSE (Baatar et al., 2013; Samoilov and Kovalenko, 1983) and (2) the association with potassic shonkinite-syenite series. The Sr and REE concentrations in apatite (Fig. 13) and the low Ti content in magnetite are similar to those in the minerals of phoscorites (Chakhmouradian et al., 2017; Krasnova et al., 2004). On the other side, in plots of Sr versus Y and Mn, and Ce/Yb_{cn} versus REE (Fig. 13 a–c), the Mushgai-Khudag apatites do not plot in the field of phoscorites, but they are in close proximity to carbonatite and jacupirangite fields, which implies their general petrological clan. However, the Mushgai-Khudag magnetite-apatite rocks are part of alkaline basic carbonatite complex and can present a specific type that associated with the alkaline shonkinite-syenite series.

In our opinion, the formation of magnetite-apatite rocks probably can be related to the liquid immiscibility process. Separation of silicate and salt melts may have occurred at the time of alkaline syenite crystallization, which is supported by the presence of magnetite-apatite schlieren in host alkaline syenites and the appearance of the Eu anomaly in apatites from magnetite-apatite rocks (see Section 7.3 of further discussion). Additional evidence is provided by the practical absence of silicates in apatite-magnetite rocks. Furthermore, Andreeva and Kovalenko (2003); Andreeva et al. (2007) observed silicate-salt liquid immiscibility in melt inclusions in minerals from rocks of the Mushgai-Khudag complex and recent experimental studies (Hou et al., 2018) demonstrated that the formation of iron oxide-apatite deposits could be explained by liquid immiscibility from the silicate melt.

Table 5
Representative chemical composition of monazite-Ce from magnetite-apatite rocks.

	1	2	3	4	5	6	7	8	9	10	11	12
Ce_2O_3	25.8	25.35	26.82	26.59	27.77	25.97	27.00	25.35	27.6	27.44	25.49	32.01
La_2O_3	16.28	16.33	16.43	17.38	17.4	15.53	16.85	15.66	16.61	16.84	13.78	17.78
Pr_2O_3	2.35	1.56	1.95	1.58	2.13	2.36	2.24	1.92	2.57	1.97	2.93	2.25
Nd_2O_3	5.70	6.39	6.44	6.61	6.14	6.59	6.16	5.81	6.35	6.36	8.12	6.50
SrO	6.67	6.65	6.61	6.52	6.39	6.23	6.37	8.72	6.53	5.82	4.21	2.57
CaO	5.39	5.30	5.09	4.49	4.27	5.55	4.86	5.11	4.48	4.67	5.58	4.45
FeO	0.90	0.73	bdl	0.86	0.82	0.80	0.60	bdl	bdl	bdl	1.57	bdl
P_2O_5	25.34	24.95	25.25	27.18	28.12	24.91	26.76	24.4	27.89	26.81	25.43	28.69
SO_3	7.84	8.47	8.19	5.87	4.74	9.21	6.94	9.94	4.72	5.12	8.12	1.97
Total	96.27	95.73	96.78	97.08	99.09	97.89	97.78	96.91	96.75	95.03	95.23	96.22
Ce apfu	0.35	0.34	0.36	0.36	0.37	0.34	0.36	0.33	0.38	0.38	0.34	0.45
La	0.22	0.22	0.22	0.24	0.24	0.21	0.22	0.21	0.23	0.24	0.18	0.25
Pr	0.03	0.02	0.03	0.02	0.03	0.03	0.03	0.03	0.04	0.03	0.04	0.03
Nd	0.07	0.08	0.08	0.09	0.08	0.08	0.08	0.07	0.08	0.09	0.11	0.09
Sr	0.14	0.14	0.14	0.14	0.14	0.13	0.13	0.18	0.14	0.13	0.09	0.06
Fe	0.03	0.02	0.00	0.03	0.03	0.02	0.02	0.00	0.00	0.00	0.05	0.00
Ca	0.21	0.21	0.20	0.18	0.17	0.21	0.19	0.20	0.18	0.19	0.22	0.18
P	0.79	0.77	0.78	0.85	0.88	0.76	0.82	0.74	0.88	0.86	0.78	0.94
S	0.22	0.23	0.22	0.16	0.13	0.25	0.19	0.27	0.13	0.15	0.22	0.06

Note: apfu – atom per formula units are based on 4 oxygens.

Another factor that confirms the possibility of the existence of silicate-salt immiscibility is a high amount of fluorine in the residual melt that could facilitate the immiscibility, and it is well justified by the experimental data (Hou et al., 2017; Lester et al., 2013). Some doubts arise from the fact that we did not observe the silicate-salt immiscibility in the melt inclusions in apatite of the Mushgai-Khudag magnetite-apatite rocks. This discrepancy can be explained by the fact that Andreeva and Kovalenko (2003); Andreeva et al. (2007) observed silicate-salt liquid immiscibility in apatite from the early formed alkaline silicate rocks of the complex.

7.2. Evolution of the melt/brine and the features of hydrothermal alterations

Based on the study of melt inclusions (Andreeva and Kovalenko, 2003) and geochemical data (Samoilov and Kovalenko, 1983), it was suggested that nephelinite magma was parental for the alkaline rocks of the Mushgai-Khudag complex. According to melt inclusion data (Andreeva and Kovalenko, 2003), the magma was heterogeneous and consisted of silicate and silicate-phosphate melts: the crystallization of the nephelinite magma began under dry conditions at a temperature of 1220 °C. The whole series of alkaline rocks has been formed by fractional crystallization process at temperatures that gradually decreased from 1220 to 850 °C (Andreeva and Kovalenko, 2003; Samoilov et al., 1988).Our data on melt inclusion in the apatite of magnetite-apatite rocks testify that the rocks were formed from the salt melt, with high phosphate and sulfate contents. The rocks were crystallized during the last stages of magmatic differentiation, at a temperature of approximately 830–850 °C. Further evolution of the salt melt led to the formation of the carbonate-(fluoride)-chloride-sulfate brine-melts at a temperature of approximately 500–580 °C.

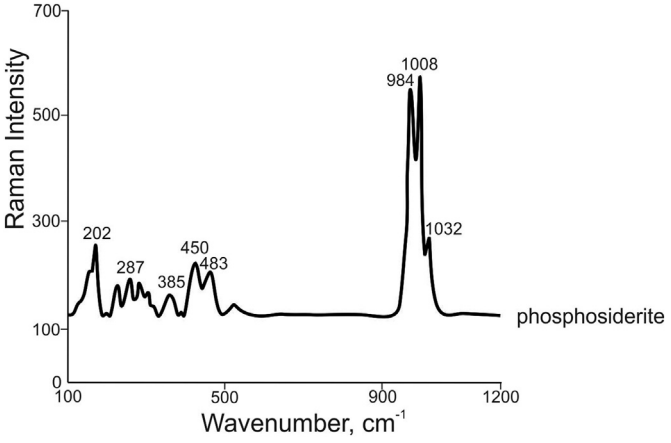

Fig. 9. Raman spectra of phosphosiderite from magnetite-apatite rocks.

The composition of the brine-melt crystal-fluid inclusions is characterized by the high concentrations of CO_2, LREE (manifested by the monazite daughter phase), Fe (in silicate phase and haematite daughter crystals), Ba and Sr (Ba-celestite) and F (fluorite). Such brine-melts were probably responsible for the F-Ba-Sr-REEs mineralization at the temperature of 500–580 °C and were characterized by the highly oxidized state, which was evidenced by the formation of haematite, with a high activity of the SO_4^{2-}-ligand, which was indicated by the broad occurrence of abundant anhydrite and celestite daughter-phases.

The high activity of the sulfate-ion in the formation of the magnetite-apatite rocks is reflected by their mineralogy. Strong evidence comes from the high SO_3 concentrations in fluorapatite. Experimental data (Katsura and Nagashima, 1974; Luhr et al., 1984) testify to the dependence of SO_3 concentration in minerals in the amount of SO_3 in the melts. In addition, Parat and Holtz (2004, 2005) experimentally confirmed that the presence of sulfur in the melt, under oxidizing conditions, increases the solubility of phosphorus and the sulfur partition coefficients between apatite and melt depend on the temperature and on the sulfur content in the melt. Natural comparisons include SO_3-rich magmatic apatite from the rocks of the carbonatite complexes of the Western Transbaikalia (Doroshkevich et al., 2003), as well as carbonatites from Kandaguba and Vuoriyarvi (Bulakh et al., 2000; Kukharenko et al., 1965). As mentioned above, the monazite from the Mushgai-Khudag complex has very high SO_3 content in comparison with that of the apatite, in spite of the fact that the apatite structure has a high capacity for substitutions involving SO_4^{2-}. Thus, we suggest that the influence of sulfur was actively continued at the hydrothermal stage, when monazite was formed. Similar S-rich monazite was previously observed in Yakutia (Chakhmouradian and Mitchell, 1999), Carpathians (Ondrejka et al., 2007) and at the Shellgaden district of the Eastern Alps (Krenn et al., 2011). The authors concluded that the S-rich phosphates are indicators of S-rich crystallizing environments. Our investigations and the occurrence of the hydrothermal S-bearing monazite together with sulfate mineralization, imply that the LREE are highly soluble in such environments and the solubility of REE probably increases with the high activity of the $(SO_4)^{2-}$-ligand. Enkhbayar et al.

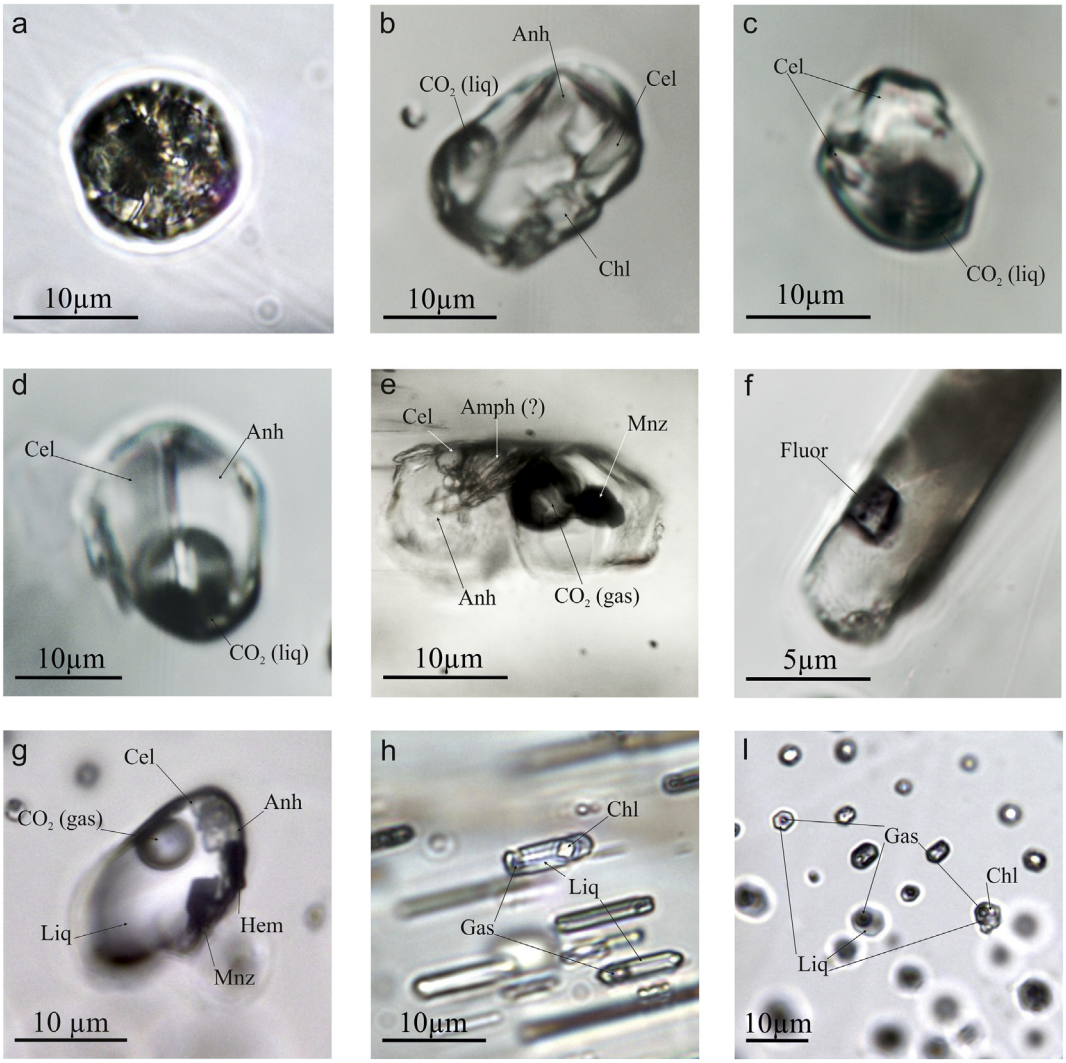

Fig. 10. Inclusions in apatite of the magnetite-apatite rocks at the Mushgai-Khudag complex. Melt inclusion (a) and brine-melt inclusions (b-e); the xenogeneic fluorite phase in the salt-fluid inclusion (f). Crystal-fluid inclusions of unaltered (g) and hydrothermal altered rocks (h, i). Abbreviation: Anh – anhydrite, Cel – celestite, Amph – amphibole, Mnz – monazite, Fluor – fluorite, Hem – haematite, Chl – chloride phase (NaCl/KCl), CO_2 (liq) – liquid CO_2, CO_2 (gas) - gaseous CO_2, Liq – liquid phase, Gas – gaseous phase.

(2016) also suggested that sulfate ligand was responsible for the REE mobility at Mushgai-Khudag.

The presence of magmatic celestite, anhydrite, and barite is typical for the Mushgai-Khudag alkaline complex as well as for the carbonatites of the West Transbaikalia. These minerals were found in daughter phases in the brine-melt inclusions of minerals from the carbonatites of the Transbaikalia and Tuva regions (Doroshkevich and Ripp, 2004; Prokopyev et al., 2016). As noted above, the significant role of the sulfate ion that manifested at the hydrothermal stages is characterized by the formation of gypsum, barite, sulfides (pyrite) and monazite-Ce enriched in SO_3. At medium hydrothermal temperatures of approximately 400–250 °C (according to the crystal-fluid water-salt inclusion data in the apatite and fluorite rocks), the sulfate acted as a strong oxidant of the fluid-transported metal cations. The hydrothermal-metasomatic alteration of the apatite crystals were characterized by the formation of gypsum, monazite-Ce, and phosphosiderite. The processes of the hydrothermal-metasomatic alteration can be summarized by the following chemical reactions:

- $Ca_5(PO_4)_3F + 5SO_4^{2-} + 5nH_2O \rightarrow 3PO_4^{3-} + 5CaSO_4{}^*nH_2O\downarrow + F^-$
- $Fe_2O_3 + 3H_2SO_4 = Fe_2(SO_4)_3 + 3H_2O$
- $Fe_2(SO_4)_3 + 2PO_4^{3-} + 2H_2O \rightarrow 2FePO_4{}^*H_2O\downarrow + 3SO_4^{2-}$

The high chemical activity of sulfur in the hydrothermal solution led to dissolution of apatite and the release of phosphate and fluorine ions. The fluorine ions could bind calcium and form fluorite. Magnetite was replaced by haematite, part of which, upon interaction with the aggressive sulfate ion, formed an unstable soluble salt, which then formed phosphosiderite. Possibly, there was some additional influx of iron from the hydrothermal solution.

According to the fluid inclusion data, the fluids of the Fe-F-Ba-Sr-REE mineralization at the Mushgai-Khudag complex have the oxidized state of coexisting sulfate-sulfide. The oxidized ore-forming fluids were established in the many alkaline complexes of the Aldan shield, Gorny Altay lamprophyres, West Transbaikalia and Tuva region carbonatites (Borisenko et al., 2011; Doroshkevich and Ripp, 2004; Prokopyev et al., 2016, 2017, 2018). Moreover, the similarity with the above-listed alkaline complexes, the chloride low-concentrated (9.2–6.4 wt.% NaCl-eq.) fluid solutions of the NaCl-H_2O-CO_2 composition and the decrease from 250 to 150 °C temperature, were responsible for the late stages of hydrothermal mineralization.

It is possible that the source of phosphorus and sulfur could be the Palaeozoic strata. However, according to a detailed geological study (Baskina et al., 1978; Samoilov and Kovalenko, 1983), the Palaeozoic country rocks are represented by limestones and terrigenous deposits, lavas and tuff breccias of andesite and andesite-dacite porphyries,

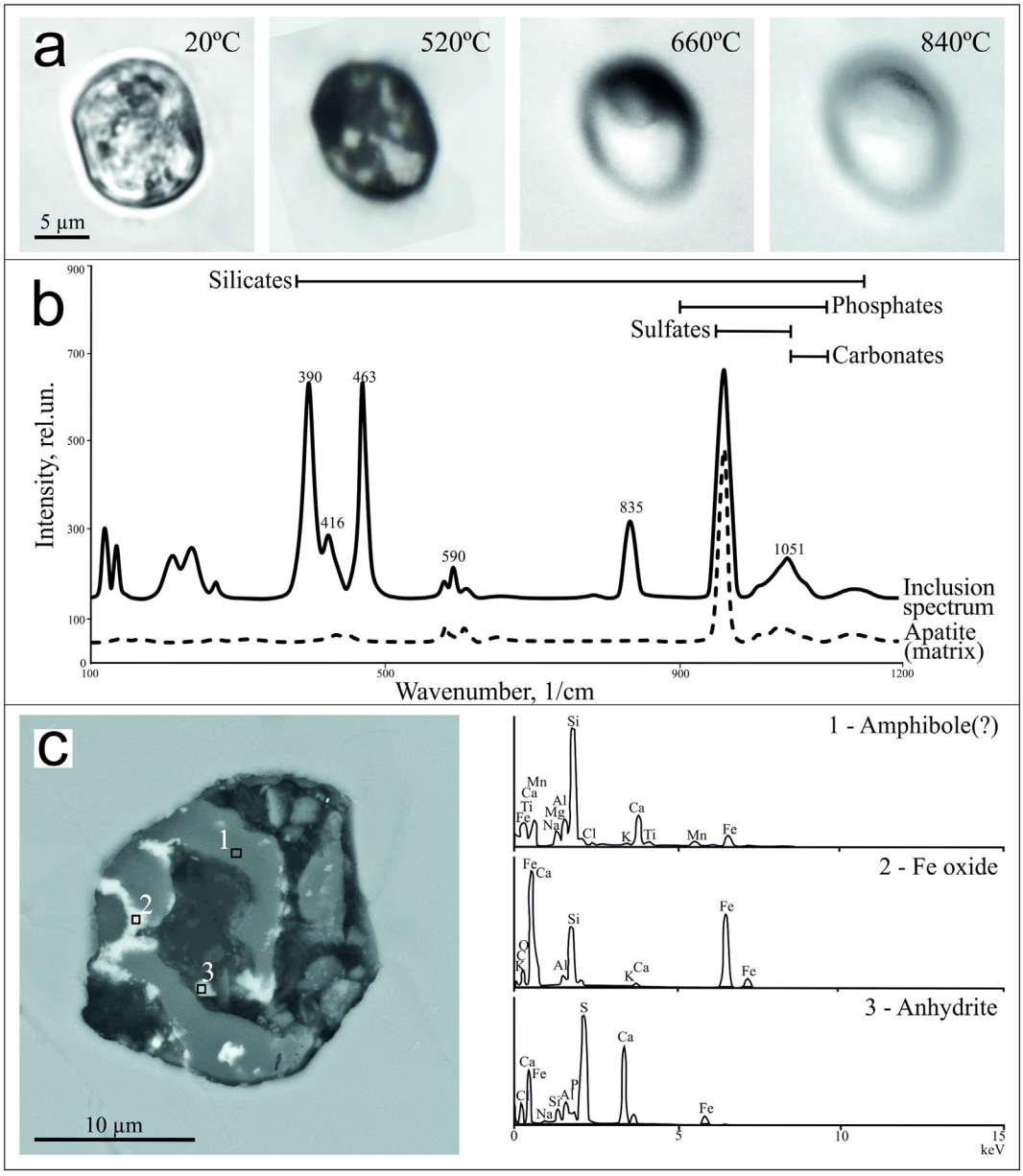

Fig. 11. Homogenization process of the melt inclusion in the apatite crystal of the magnetite-apatite rocks (a); results of Raman-spectroscopy of the melt inclusion and Raman vibrational regions of silicates, phosphates, sulfates and carbonates according to Frezzotti et al. (2012) (b); SEM-photo and spectra of the investigated daughter-phases (c).

tuffaceous sandstones and tuff gravelstones. In addition, the oxygen isotopic data of the Mushgai-Khudag magnetite-apatite rocks do not show any evidence of the significant role of crustal material, that along with geochemical and melt inclusion data, confirms the initial P- and S- enrichment of the primary nephelinite melt. Kogarko and Ryabchikov (1983) observed that phosphorus is concentrated (up to 12.5 wt.% P_2O_5) with alkalis in low-degree primary nephelinite magmas.

7.3. The behavior of REE during the system evolution

As demonstrated by the REE chondrite-normalized plots (Fig. 7), the concentrations of REEs in apatite increase from shonkinites to alkaline syenites, and a negative Eu anomaly appears along with the increase. Such a trend probably results from fractional crystallization involving feldspar fractionation. The subsequent increase in REE concentrations in apatite from magnetite-apatite rocks and the preservation of the negative Eu anomaly implies that the rocks are also a product of magmatic fractional crystallization of the parental alkaline silicate phosphorus-rich melt.

There may be two reasons for the further increase in the REE concentrations and the disappearance of the Eu anomaly in apatite from the hydrothermally altered magnetite-apatite rocks:

1) influx of large amounts of REEs by hydrothermal solutions without the Eu anomaly.
2) influx of REEs coupled with the reduction of Eu^{3+} to Eu^{2+}.

In the first case, REEs brought by the hydrothermal fluid should come from a source that did not experience feldspar fractionation. The possible sources include the country sandstones, carbonatites and/or alkaline silicate rocks, e.g., shonkinites. According to (Andreeva et al., 2007; Andreeva and Kovalenko, 2003), carbonatites at Mushgai-Khudag formed by silicate–carbonate liquid immiscibility, taking into account the experimentally determined liquid–liquid partition coefficients (Martin et al., 2012, 2013; Veksler et al., 1998, 2012), those carbonatites

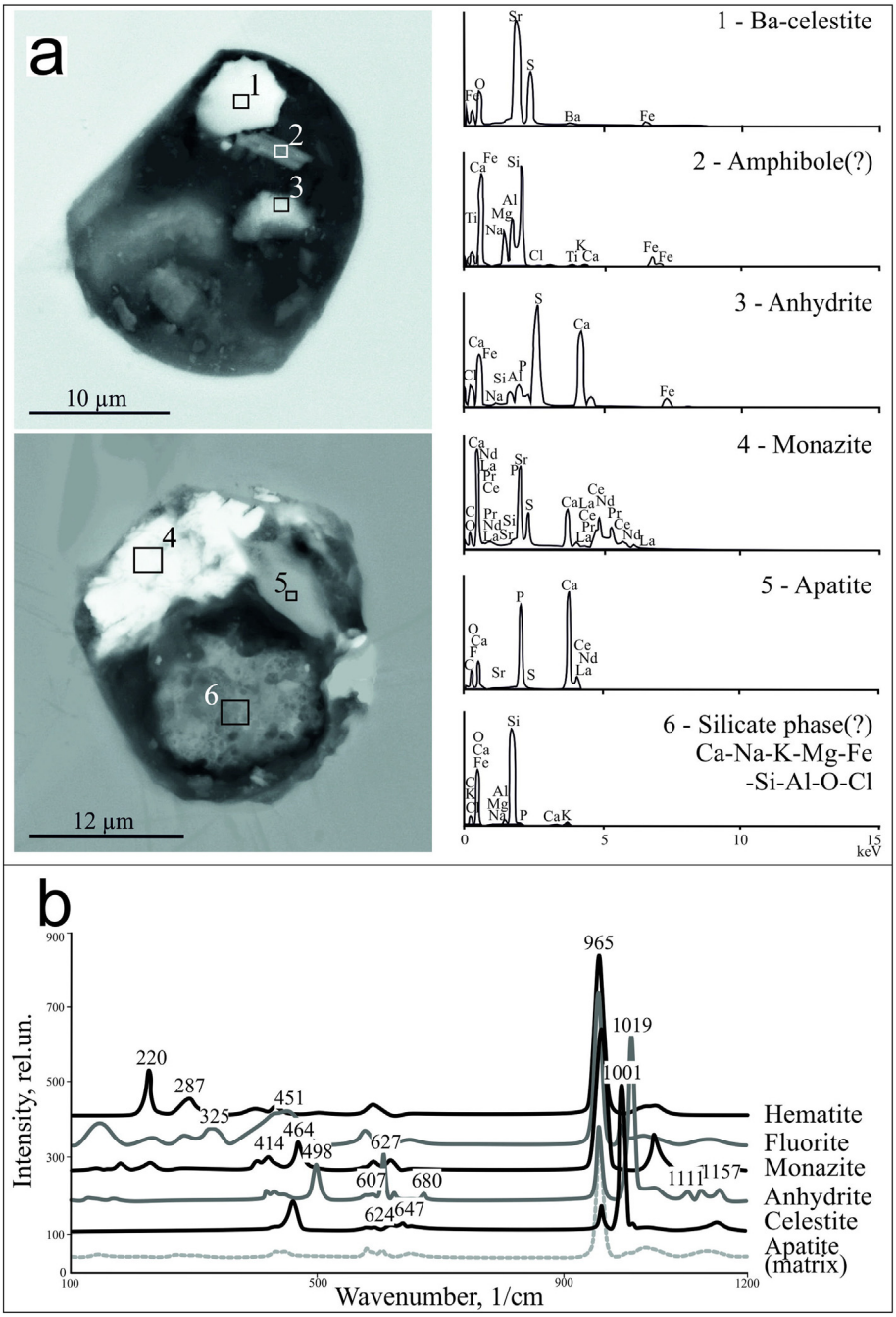

Fig. 12. Phase composition of brine-melt crystal-fluid inclusions in apatite of the magnetite-apatite rocks: SEM analyses of opened inclusions (a) and Raman-data of the crystal daughter-phases of the inclusions (b).

may have contained high REE concentrations. Due to the further evolution of carbonatitic magma, the residual brine-melt may have become even more enriched in REEs. One should point out, however, that the Mushgai-Khudag carbonatites do not host any significant REE mineralization (Baskina et al., 1978; Ontoev et al., 1979; Samoilov and Kovalenko, 1983). Therefore, shonkinites appear to be the most likely source of REEs for hydrothermal fluid.

The second possibility that requires Eu^{3+} reduction to Eu^{2+} also appears to be plausible. The Eu^{3+}/Eu^{2+} redox equilibrium in hydrothermal environments has to be considered as a function of temperature, pressure, the concentration of ligands and pH (e.g., Bau, 1991; Liu et al., 2017; Migdisov et al., 2016). Michard (1989) points to an Eu^{3+} reduction in a chloride-rich solution with pH <7 in the natural geothermal fields. In addition, the reduction of Eu^{3+} to Eu^{2+} has been theoretically demonstrated in a hydrothermal solution at temperatures between 100°C and 250 °C, with SO_4^{2-}/H_2S, or in a magnetite-haematite equilibrium (Bau, 1991; Liu et al., 2017). The Eu^{3+} reduction is supported by sulfide and sulfate coexistence in the Mushgai-Khudag rocks, homogenization temperature of fluid inclusions in altered apatite, and a high activity of ligands (SO_3^{2-}, HPO_3^{2-}, CO). Indirectly, the formation of phosphosiderite after apatite can confirm HPO_3^{2-} as the possible reduced component. However, according to our fluid inclusions studies, fluid compositions at Mushgai-Khudag are complex and have evolved from carbonate-chloride-sulfate mixtures to predominantly chloride. It is difficult to reconstruct the oxidation–reduction reactions that have been responsible for the Eu^{3+} reduction.

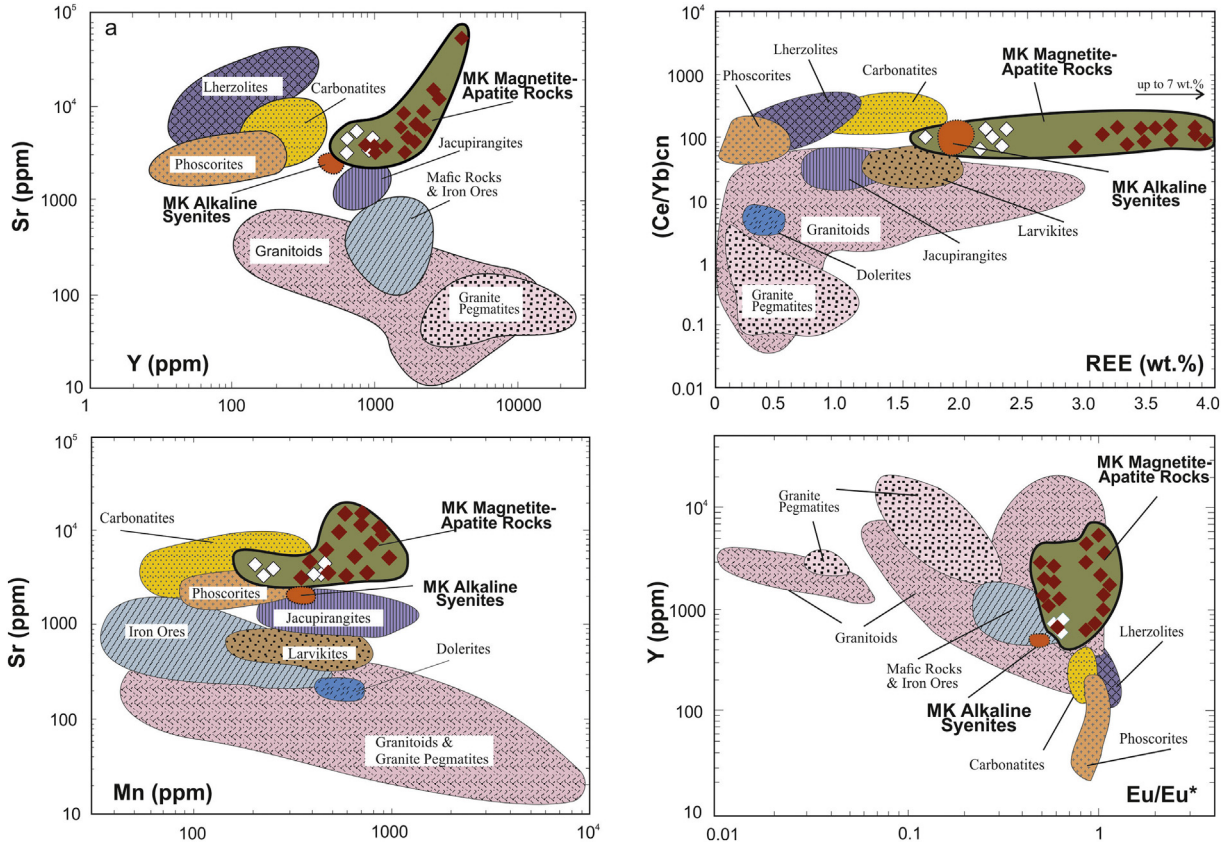

Fig. 13. Compositional fields of apatite from different rock types, proposed as discriminant plots, after Belousova et al., 2002. Compositional fields of phoscorites were inferred from the analyses of apatites from Kovdor phoscorites and Aley apatitites (Chakhmouradian et al., 2017). White rhombs correspond to apatite from unaltered magnetite-apatite rocks, dark rhombs correspond to apatites from altered magnetite-apatite rocks.

8. Conclusions

The magnetite-apatite rocks are the product of silicate-salt liquid immiscibility from highly evolved parental alkaline silicate melt. The evolution of the salt melt to the brine melt of the silicate–carbonate-(fluoride)-chloride-sulfate composition, the high activity of the SO_4^{2-}-ligand and a significant enrichment of the rocks in REEs led to the formation of the barite, celestite and monazite-Ce. The formation of gypsum, phosphosiderite and sulfate-rich monazite-Ce after apatite occured at the late hydrothermal stage under the actively continued influence of sulfur. Then, the hydrothermal fluid from highly concentrated carbonate-chloride-sulfate brine evolved to a predominantly chloride composition.

Acknowledgments

Geochemical and isotopic studies of the rocks were supported by the research project of the Institute of Geology and Mineralogy SB RAS, No 0330-2016-0002. Mineralogical investigations were carried out using funds from grant of Russian Government (project no. 14.Y26.31.0012).

References

Andreev, G.V., Khubanov, V.B., 2005. Chemical composition of the major minerals in ores of (Apatite) deposit, the Mushugai ore field (Mongolia). Not. Russian Mineral. Soc. 134 (2), 52–56 (in Russian).

Andreeva, I.A., 2000. Silicate, silicate-salt and salt magmas of the alkaline carbonate-containing complex Mushugai-Khuduk, southern Mongolia (melt inclusions study data). PhD Thesis. IGEM, Moscow (in Russian).

Andreeva, I.A., Kovalenko, V.I., 2003. Magma compositions and genesis of the rocks of the Mushugai-Khuduk carbonatite-bearing alkaline complex (southern Mongolia): evidence from melt inclusions. Period. Mineral. 72, 95–105.

Andreeva, I.A., Naumov, V.B., Kovalenko, V.I., Kononkova, N.N., 1998. Fluoride-sulfate and chloride-sulfate salt melts of the carbonatite-bearing complex Mushugai-Khuduk, Southern Mongolia. Petrology 6 (3), 284–292.

Andreeva, I.A., Kovalenko, V.I., Naumov, V.B., 2007. Silicate-salt (sulfate) liquid immiscibility: a study of melt inclusions in minerals of the Mushugai-Khuduk carbonatite-bearing complex (southern Mongolia). Acta Petrol. Sin. 23, 73–82.

Baatar, M., Ochir, G., Kynicky, J., Iizumi, S., Comin-Chiaramonti, P., 2013. Some notes on the Lugiin Gol, Mushgai Khudag and Bayan Khoshuu alkaline complexes, southern Mongolia. Int. J. Geosci. 4 (8), 1200–1214. https://doi.org/10.4236/ijg.2013.48114.

Baskina, V.A., Volchanskaya, I.K., Kovalenko, V.I., Samoilov, V.S., Vladykin, N.V., Goreglyad, A.V., 1978. The potassic alkaline volcanic-plutonic massif at Mushugai-Khuduk in Southern Mongolia and related mineralization. Soviet Geol. 4, 86–99 (in Russian).

Bau, M., 1991. Rare-earth element mobility during hydrothermal and metamorphic fluid-rock interaction and the significance of the oxidation state of europium. Chem. Geol. 93 (3–4), 219–230. https://doi.org/10.1016/0009-2541(91)90115-8.

Belousova, E.A., Griffin, W.L., O'Reilly, S.Y., Fisher, N.I., 2002. Apatite as an indicator mineral for mineral exploration: trace-element compositions and their relationship to host rock type. J. Geochem. Explor. 76 (1), 45–69. https://doi.org/10.1016/S0375-6742(02)00204-2.

Bolonin, A.V., 2007. Carbonatite complex ores of central Tuva and the prospects for their development. Ores Metals 6, 16–26 (in Russian).

Bookstrom, A.A., 1995. Magmatic features of iron ores of the Kiruna type in Chile and Sweden; ore textures and magnetite geochemistry; discussion. Econ. Geol. 90 (2), 469–473. https://doi.org/10.2113/gsecongeo.90.2.469.

Borisenko, A.S., Borovikov, A.A., Vasyukova, E.A., Pavlova, G.G., Ragozin, A.L., Prokopyev, I. R., Vladykin, N.V., 2011. Oxidized magmatogene fluids: metal-bearing capacity and role in ore formation. Russ. Geol. Geophys. 52 (1), 182–206. https://doi.org/10.1016/j.rgg.2010.12.011.

Bulakh, A.G., Nesterov, A.R., Zaitsev, A.N., Pilipiuk, A.N., Wall, F., Kirillov, A.S., 2000. Sulfur-containing monazite-(Ce) from late-stage mineral assemblages at the Kandaguba and Vuoriyarvi carbonatite complexes, Kola peninsula, Russia. Neues Jahrbuch Fur Mineralogie Monatshefte 5, 217–233.

Bulnaev, K.B., Posokhov, V.F., 1995. Isotopic-geochemical data on the nature and age of endogenous carbonate rocks of Transbaikalia. Geochemistry 2, 189–195 (in Russian).

Chakhmouradian, A.R., Mitchell, R.H., 1999. Niobian ilmenite, hydroxylapatite and sulfatian monazite; alternative hosts for incompatible elements in calcite kimberlite from Internatsional'naya, Yakutia. Can. Mineral. 37 (5), 1177–1189.

Chakhmouradian, A.R., Reguir, E.P., Zaitsev, A.N., Couëslan, C., Xu, C., Kynický, J., Mumin, H., Yang, P., 2017. Apatite in carbonatitic rocks: Compositional variation, zoning,

element partitioning and petrogenetic significance. Lithos 274, 188–213. https://doi.org/10.1016/j.lithos.2016.12.037.
Charlier, B., Sakoma, E., Sauvé, M., Stanaway, K., Vander Auwera, J., Duchesne, J.C., 2008. The Grader layered intrusion (Havre-Saint-Pierre Anorthosite, Quebec) and genesis of nelsonite and other Fe-Ti-P ores. Lithos 101 (3–4), 359–378. https://doi.org/10.1016/j.lithos.2007.08.004.
Daliran, F., 2002. Kiruna-type iron oxide-apatite ores and apatitites of the Bafq district, Iran, with an emphasis on the REE geochemistry of their apatites. In: Porter, T.M. (Ed.), Hydrothermal Iron Oxide Copper-Gold and Related Deposits: A Global Perspective (2). PGS Publishing, Adelaide, pp. 303–320.
Demény, A., Kele, S., Siklosy, Z., 2010. Empirical equations for the temperature dependence of calcite-water oxygen isotope fractionation from 10 to 70 °C. Rapid Commun. Mass Spectrom. 24 (24), 3521–3526. https://doi.org/10.1002/rcm.4799.
Doroshkevich, A.G., Ripp, G.S., 2004. Estimation of the conditions of formation of REE-carbonatites in Western Transbaikalia. Russ. Geol. Geophys. 45 (4), 492–500.
Doroshkevich, A.G., Ripp, G.S., 2009. Isotopic systematics of the rocks of the Khalyuta carbonatite complex of western Transbaikalia. Geochem. Int. 47 (12), 1198. https://doi.org/10.1134/S0016702909120040.
Doroshkevich, A.G., Kobylkina, O.V., Ripp, G.S., 2003. Role of sulfates in the formation of carbonatites in the Western Transbaikal Region. Dokl. Earth Sci. 388, 131–134.
Doroshkevich, A.G., Ripp, G.S., Viladkar, S.G., Vladykin, N.V., 2008. The Arshan REE carbonatites, southwestern Transbaikalia, Russia: mineralogy, paragenesis and evolution. Can. Mineral. 46 (4), 807–823. https://doi.org/10.3749/canmin.46.4.807.
Doroshkevich, A.G., Ripp, G.S., Moore, K.R., 2010. Genesis of the Khaluta alkaline-basic Ba-Sr carbonatite complex (West Transbaikala, Russia). Mineral. Petrol. 98 (1–4), 245–268. https://doi.org/10.1007/s00710-009-0063-4.
Doroshkevich, A.G., Veksler, I.V., Izbrodin, I.A., Ripp, G.S., Khromova, E.A., Posokhov, V.F., Travin, A.V., Vladykin, N.V., 2016. Stable isotope composition of minerals in the Belaya Zima plutonic complex, Russia: implications for the sources of the parental magma and metasomatizing fluids. J. Asian Earth Sci. 116, 81–96. https://doi.org/10.1016/j.jseaes.2015.11.011.
Duchesne, J.C., Liégeois, J.P., 2015. The origin of nelsonite and high-Zr ferrodiorite associated with Proterozoic anorthosite. Ore Geol. Rev. 71, 40–56. https://doi.org/10.1016/j.oregeorev.2015.05.005.
Dunworth, E.A., Bell, K., 2001. The Turiy massif, Kola Peninsula, Russia: isotopic and geochemical evidence for multi-source evolution. J. Petrol. 42 (2), 377–405. https://doi.org/10.1093/petrology/42.2.377.
Egorov, L.S., 1992. Phoscorites of Maymeicha-Kotui ijolite-carbonatite complex. Not. All-Russian Mineral. Soc. 121 (3), 13–26 (in Russian).
Enkhbayar, D., Seo, J., Choi, S.G., Lee, Y.J., Batmunkh, E., 2016. Mineral chemistry of REE-rich apatite and sulfur-rich monazite from the Mushgai Khudag, Alkaline Volcanic-Plutonic Complex, South Mongolia. Int. J. Geosci. 7 (1), 20–31. https://doi.org/10.4236/ijg.2016.71003.
Eriksson, S.C., 1989. Phalaborwa: a saga of magmatism, metasomatism and miscibility. In: Bell, K. (Ed.), Carbonatites: genesis and evolution. Unwin Hyman, London, pp. 221–254.
Fleischer, M., 1978. Relative proportions of the lanthanides in minerals of the bastnaesite group. Can. Mineral. 16, 361–363.
Force, E.R., 1991. Geology of titanium-mineral deposits. Geol. Soc. Am. Spec. Pap., 259 https://doi.org/10.1130/SPE259-p1.
Frezzotti, M.L., Tecce, F., Casagli, A., 2012. Raman spectroscopy for fluid inclusion analysis. J. Geochem. Explor. 112, 1–20. https://doi.org/10.1016/j.gexplo.2011.09.009.
Frietsch, R., Perdahl, J.A., 1995. Rare earth elements in apatite and magnetite in Kiruna-type iron ores and some other iron ore types. Ore Geol. Rev. 9 (6), 489–510. https://doi.org/10.1016/0169-1368(94)00015-G.
Gittins, J., 1966. Summaries and bibliographies of carbonatite complexes. In: Gittins, J., Tuttle, O.F. (Eds.), Carbonatites. Wiley Interescience, New York, pp. 417–570.
Harlov, D.E., Förster, H.J., Schmidt, C., 2003. High PT experimental metasomatism of a fluorapatite with significant britholite and fluorellestadite components: implications for LREE mobility during granulite-facies metamorphism. Mineral. Mag. 67 (1), 61–72. https://doi.org/10.1180/0026461036710084.
Harmer, R.E., 2000. Mineralisation of the Phalaborwa complex and the carbonatite connection in iron oxide-Cu-Au-U-REE deposits. In: Porter, T.M. (Ed.), Hydrothermal iron oxide copper-gold and related deposits: a global perspective. 1. Adelaide, PGS Publishing, pp. 331–340.
Hildebrand, R.S., 1986. Kiruna-type deposits; their origin and relationship to intermediate subvolcanic plutons in the Great Bear magmatic zone, Northwest Canada. Econ. Geol. 81 (3), 640–659. https://doi.org/10.2113/gsecongeo.81.3.640.
Hoefs, J., 2015. Stable Isotope Geochemistry. Springer International Publishing, AG, Basel https://doi.org/10.1007/978-3-319-19716-6.
Hou, T., Zhang, Z., Kusky, T., 2011. Gushan magnetite-apatite deposit in the Ningwu basin, Lower Yangtze River Valley, SE China: hydrothermal or Kiruna-type? Ore Geol. Rev. 43 (1), 333–346. https://doi.org/10.1016/j.oregeorev.2011.09.014.
Hou, T., Charlier, B., Namur, O., Schütte, P., Schwarz-Schampera, U., Zhang, Z., Holtz, F., 2017. Experimental study of liquid immiscibility in the Kiruna-type Vergenoeg iron-fluorine deposit, South Africa. Geochim. Cosmochim. Acta 203, 303–322. https://doi.org/10.1016/j.gca.2017.01.025.
Hou, T., Charlier, B., Holtz, F., Veksler, I., Zhang, Z., Thomas, R., Namur, O., 2018. Immiscible hydrous Fe-Ca-P melt and the origin of iron oxide-apatite ore deposits. Nat. Commun. 9, 1415. https://doi.org/10.1038/s41467-018-03761-4.
Issa Filho, A., Lima dos Santos, P.R.A., Souza, O.M., 1984. Aspects of the geology of the Barreiro carbonatitic complex, Araxá, MG, Brazil. Carbonatitic Complexes of Brazil: Geology. Mineração (Department of Geology), Sao Paulo, Companhia Brasileira de Metalurgia e.
Katsura, T., Nagashima, S., 1974. Solubility of sulfur in some magmas at 1 atmosphere. Geochim. Cosmochim. Acta 38 (4), 517–531.
Kogarko, L.N., Ryabchikov, I.D., 1983. Phosphorus in mantle melting processes. Rep. Acad. Sci. USSR 269 (5), 1192–1194 (in Russian).
Kogarko, L.N., Plant, D.A., Henderson, C.M.B., Kjarsgaard, B.A., 1991. Na-rich carbonate inclusions in perovskite and calzirtite from the Guli intrusive Ca-carbonatite, polar Siberia. Contrib. Mineral. Petrol. 109 (1), 124–129. https://doi.org/10.1007/BF00687205.
Kovalenko, V.I., Yarmolyuk, V.V., Kovach, V.P., Kotov, A.B., Kozakov, I.K., Salnikova, E.B., Larin, A.M., 2004. Isotope provinces, mechanisms of generation and sources of the continental crust in the Central Asian mobile belt: geological and isotopic evidence. J. Asian Earth Sci. 23 (5), 605–627. https://doi.org/10.1016/S1367-9120(03)00130-5.
Krasnova, N.I., Petrov, T.G., Balaganskaya, E.G., Garcia, D., Moutte, J., Zaitsev, A.N., Wall, F., 2004. Introduction to phoscorites: occurrence, composition, nomenclature and petrogenesis. In: Wall, F., Zaitsev, A.N. (Eds.), Phoscorites and Carbonatites from Mantle to Mine: the Key Example of the Kola Alkaline Province. The Mineralogical Society of Great Britain and Ireland, London, pp. 45–74.
Krenn, E., Putz, H., Finger, F., Paar, W.H., 2011. Sulfur-rich monazite with high common Pb in ore-bearing schists from the Schellgaden mining district (Tauern Window, Eastern Alps). Mineral. Petrol. 102 (1–4), 51–62. https://doi.org/10.1007/s00710-011-0170-x.
Krmíček, L., Kynický, J., Krmíčova, M., 2010. Finding of limestone-alkaline lamprophy in the association of alkaline rocks and Mushugai Khuduk Carbonatites in Mongolia. Geological Surveys Reports for 2009. Czech Geological Survey, Praha, pp. 266–270 (in Czech).
Kukharenko, A.A., Il'inskii, G.A., Ivanova, T.N., Bulakh, A.G., Bagdasarov, E.A., Sergeev, A.S., Abakumova, N.B., 1965. The Caledonian Complex of Ultrabasic and Alkaline Rocks and Carbonatites of the Kola Peninsula and Northern Karelia. Nedra, Moscow (in Russian).
Kuzmin, M.I., Yarmolyuk, V.V., 2014. Mantle plumes of Central Asia (Northeast Asia) and their role in forming endogenous deposits. Russ. Geol. Geophys. 55 (2), 120–143. https://doi.org/10.1016/j.rgg.2014.01.002.
Kynicky, J., Chakhmouradian, A., 2011. Exotic rocks and REE apatite mineralization of Ulugei Khid massif in the Mongolia. Geological Surveys Reports for 2010, Czech Geological Survey, Praha, pp. 205–210 (in Czech with English abstract).
Kynický, J., Samec, P., 2005. Hydrothermally-metasomatic and exsolution-like mineralization of the carbonatites from the selected localities at Gobi. Mongolian Geosci. 27, 52–56.
Le Bas, M.J., 1989. Nephelinitic and basanitic rocks. J. Petrol. 30 (5), 1299–1312. https://doi.org/10.1093/petrology/30.5.1299.
Le Maitre, R.W., Streckeisen, A., Zanettin, B., Le Bas, M.J., Bonin, B., Bateman, P., 2002. Igneous Rocks: A Classification and Glossary of Terms. second ed. Cambridge University Press, Cambridge https://doi.org/10.1017/CBO9780511535581.
Lester, G.W., Clark, A.H., Kyser, T.K., Naslund, H.R., 2013. Experiments on liquid immiscibility in silicate melts with H_2O, P, S, F and Cl: implications for natural magmas. Contrib. Mineral. Petrol. 166 (1), 329–349. https://doi.org/10.1007/s00410-013-0878-1.
Liu, W., Etschmann, B., Migdisov, A., Boukhalfa, H., Testemale, D., Müller, H., Hazemann, J.-L., Brugger, J., 2017. Revisiting the hydrothermal geochemistry of europium (II/III) in light of new in-situ XAS spectroscopy results. Chem. Geol. 459, 61–74. https://doi.org/10.1016/j.chemgeo.2017.04.005.
Luhr, J.F., Carmichael, I.S., Varekamp, J.C., 1984. The 1982 eruptions of El Chichón Volcano, Chiapas, Mexico: mineralogy and petrology of the anhydritebearing pumices. J. Volcanol. Geotherm. Res. 23 (1–2), 69–108. https://doi.org/10.1016/0377-0273(84)90057-X.
Martin, L.H.J., Schmidt, M.W., Hannes, B., Mattsson, H.B., Ulmer, P., Hametner, K., Günther, D., 2012. Element partitioning between immiscible carbonatite-kamafugite melts with application to the Italian ultrapotassic suite. Chem. Geol. 320-321, 96–112. https://doi.org/10.1016/j.chemgeo.2012.05.019.
Martin, L.H.J., Schmidt, M.W., Mattson, H.B., Guenther, D., 2013. Element partitioning between immiscible carbonatite and silicate melts from dry and H_2O-bearing systems at 1–3 GPa. J. Petrol. 54, 2301–2338. https://doi.org/10.1093/petrology/egt048.
Michard, A., 1989. Rare earth element systematics in hydrothermal fluids. Geochim. Cosmochim. Acta 53 (3), 745–750. https://doi.org/10.1016/0016-7037(89)90017-3.
Migdisov, A., Williams-Jones, A.E., Brugger, J., Caporuscio, F.A., 2016. Hydrothermal transport, deposition, and fractionation of the REE: Experimental data and thermodynamic calculations. Chem. Geol. 439, 13–42. https://doi.org/10.1016/j.chemgeo.2016.06.005.
Mitchell, R.H., 2005. Carbonatites and carbonatites and carbonatites. Can. Mineral. 43 (6), 2049–2068. https://doi.org/10.2113/gscanmin.43.6.2049.
Nikiforov, A.V., Yarmolyuk, V.V., 2004. Late Mesozoic central Asian carbonatite province. In: Sklyarov, E.V. (Ed.), Geodynamic Evolution of the Lithosphere of the Central Asian Mobile Belt. Institute of Geography V.B. Sochava SB RAS, Irkutsk, pp. 47–49 (in Russian).
Nikiforov, A.V., Yarmolyuk, V.V., Pokrovsky, B.G., Kovalenko, V.I., Ivanov, V.G., Ripp, G.S., 1998. Isotope composition of oxygen, carbon and sulfur of rocks of the Khalyutinsky volcanic carbonatite complex (Western Transbaikalia). Dokl. Earth Sci. 363 (6), 815–818 (in Russian).
Nikiforov, A.V., Bolonin, A.V., Chugaev, A.V., Lykhin, D.A., Pokrovsky, B.G., Sugorakova, A.M., 2006. Isotope geochemistry (O, C, S, Sr) and Rb-Sr age of carbonatites in central Tuva. Geol. Ore Dep. 48 (4), 256–276. https://doi.org/10.1134/S1075701506040027.
Nikolenko, A.M., Doroshkevich, A.G., 2017. Features of mineral composition of apatite-magnetite rocks, Mushugai-Khuduk complex (Mongolia). In: Zaitsev, V.A., Ermolaeva, V.N. (Eds.), Magmatism of the Earth and related strategic metal deposits: proceedings of XXXIV International conference. GEOKHI RAS, Miass, pp. 162–165.
Nystroem, J.O., Henriquez, F., 1994. Magmatic features of iron ores of the Kiruna type in Chile and Sweden: ore textures and magnetite geochemistry. Econ. Geol. 89 (4), 820–839. https://doi.org/10.2113/gsecongeo.89.4.820.
Ondrejka, M., Uher, P., Pršek, J., Ozdín, D., 2007. Arsenian monazite-(Ce) and xenotime-(Y), REE arsenates and carbonates from the Tisovec-Rejkovo rhyolite, Western

Carpathians, Slovakia: Composition and substitutions in the (REE, Y)XO_4 system (X = P, As, Si, Nb, S). Lithos 95 (1), 116–129. https://doi.org/10.1016/j.lithos.2006.07.019.

Ontoev, D.O., Kandinov, M.N., Korytov, F., 1977. Temperatures of mineral formation of apatite-fluorite rare-earth mineralization of South Mongolia. Rep. Acad. Sci. USSR 234 (5), 1164–1166 (in Russian).

Ontoev, D.O., Luvsandanzan, B., Gundsambuu, Ts, 1979. Geology and primary mineralisation of the Mushugai F-REE deposit (Mongolia). Geol. Ore Dep. 3, 27–42 (in Russian).

Parat, F., Holtz, F., 2004. Sulfur partitioning between apatite and melt and effect of sulfur on apatite solubility at oxidizing conditions. Contrib. Mineral. Petrol. 147 (2), 201–212. https://doi.org/10.1007/s00410-004-0553-7.

Parat, F., Holtz, F., 2005. Sulfur partition coefficient between apatite and rhyolite: the role of bulk S content. Contrib. Mineral. Petrol. 150 (6), 643–651. https://doi.org/10.1007/s00410-005-0041-8.

Pichou, J.L., Pichoir, F., 1984. A new model for quantitative X-ray microanalysis. Part I: application to the analysis of homogeneous samples. La Recherche A´erospatiale 3, 13–38.

Prokopyev, I.R., Borisenko, A.S., Borovikov, A.A., Pavlova, G.G., 2016. Origin of REE-rich ferrocarbonatites in southern Siberia (Russia): implications based on melt and fluid inclusions. Mineral. Petrol. 110 (6), 845–859. https://doi.org/10.1007/s00710-016-0449-z.

Prokopyev, I.R., Doroshkevich, A.G., Ponomarchuk, A.V., Sergeev, S.A., 2017. Mineralogy, age and genesis of apatite-dolomite ores at the Seligdar apatite deposit (Central Aldan, Russia). Ore Geol. Rev. 81 (1), 296–308. https://doi.org/10.1016/j.oregeorev.2016.10.012.

Prokopyev, I.R., Doroshkevich, A.G., Redina, A.A., Obukhov, A.V., 2018. Magnetite-apatite-dolomitic rocks of Ust-Chulman (Aldan shield, Russia): Seligdar-type carbonatites? Mineral. Petrol. 112 (2), 257–266. https://doi.org/10.1007/s00710-017-0534-y.

Redina, A.A., Prokopyev, I.R., 2017. Fluid inclusion study of fluorites from the Mushugai-Khuduk carbonatite complex (Southern Mongolia). In: Pironon, J. (Ed.), Proceedings of XXIV Biennial Conference - European Current Research on Fluid Inclusions. University of Lorraine, Nancy, p. 104.

Ripp, G.S., Karmanov, N.S., Kanakin, S.V., Doroshkevich, A.G., Andreev, G.V., 2005. Cerium britholite from the Mushugai ore deposit (Mongolia). Not. Russian Mineral. Soc. 134, 90–103 (in Russian).

Ripp, G.S., Doroshkevich, A.G., Karmanov, N.S., Kanakin, S.V., 2009a. Micas from the Khaluta carbonatite deposit, western Transbaikal region. Geol. Ore Dep. 51 (8), 812–821. https://doi.org/10.1134/S1075701509080145.

Ripp, G.S., Doroshkevich, A.G., Posokhov, V.F., 2009b. Age of carbonatite magmatism in Transbaikalia. Petrology 17 (1), 73–89. https://doi.org/10.1134/S0869591109010044.

Ripp, G.S., Khodyreva, E.V., Izbrodin, I.A., Rampilov, M.O., Lastochkin, E.I., Posokhov, V.F., 2017. Genetic nature of apatite-magnetite ore in North Gurvunur deposit, western Transbaikal region. Geol. Ore Dep. 59 (5), 407–420. https://doi.org/10.1134/S1075701517050051.

Rundqvist, I.K., Baskina, V.A., Ontoev, D.O., 1995. Mushugay-Khuduk REE-Fe-F deposit in Southern Mongolia. Glob. Tecton. Metall. 5 (1–2), 41–51.

Russell, H.D., 1954. The mineralogy and petrology of the carbonatite at Loolekop, Eastern Transvaal. S. Afr. J. Geol. 57 (1), 197–208.

Sal'nikova, E.B., Yakovleva, S.Z., Nikiforov, A.V., Kotov, A.B., Yarmolyuk, V.V., Anisimova, I. V., Plotkina, Y.V., 2010. Bastnaesite: a promising U-Pb geochronological tool. Dokl. Earth Sci. 430 (1), 134–136. https://doi.org/10.1134/S1028334X10010290.

Samoilov, V.S., Kovalenko, V.I., 1983. Complexes of Alkaline Rocks and Carbonatites in South Mongolia. Nauka, Moscow (in Russian).

Samoilov, V.S., Kovalenko, V.I., Naumov, V.B., 1988. The immiscibility of silicate and salt melts during the formation of the Mushugai-Khuduk alkaline complex (South Mongolia). Geochemistry 10, 1447–1460 (in Russian).

Sharp, Z.D., 1990. A laser-based microanalytical method for the in situ determination of oxygen isotope ratios of silicates and oxides. Geochim. Cosmochim. Acta 54, 1353–1357. https://doi.org/10.1016/0016-7037(90)90160-M.

Sun, S.S., McDonough, W.S., 1989. Chemical and isotopic systematics of oceanic basalts: implications for mantle composition and processes. In: Saunders, A.D., Morry, M.J. (Eds.), Magmatism in the Ocean Basin. Vol. 42. Geological Society of London Special Publication, pp. 313–345. https://doi.org/10.114/GSL.SP.1989.042.01.19.

Tichomirowa, M., Grosche, G., Götze, J., Belyatsky, B.V., Savva, E.V., Keller, J., Todt, W., 2006. The mineral isotope composition of two Precambrian carbonatite complexes from the Kola Alkaline Province – Alteration versus primary magmatic signatures. Lithos 91 (1–4), 229–249. https://doi.org/10.1016/j.lithos.2006.03.019.

Veksler, I.V., Petibon, C., Jenner, G.A., Dorfman, A.M., Dingwell, D.B., 1998. Trace element partitioning in immiscible silicate-carbonate liquid systems: an initial experimental study using a centrifuge autoclave. J. Petrol. 39 (11–12), 2095–2104. https://doi.org/10.1093/petroj/39.11-12.2095.

Veksler, I.V., Dorfman, A.M., Dulski, P., Kamenetsky, V.S., Danyushevsky, L.V., Jeffries, T., Dingwell, D.B., 2012. Partitioning of elements between silicate melt and immiscible fluoride, chloride, carbonate, phosphate and sulfate melts, with implications to the origin of natrocarbonatite. Geochim. Cosmochim. Acta 79, 20–40. https://doi.org/10.1016/j.gca.2011.11.035.

Vladykin, N.V., 1997. Petrology and ore potential of K-alkaline rocks of the Mongol-Okhotsk magmatic area. ScD thesis. Institute of Geochemistry SB RAS, Irkutsk (in Russian).

Vladykin, N.V., 2013. Petrology and composition of rare-metal alkaline rocks in the South Gobi Desert (Mongolia). Russ. Geol. Geophys. 54 (4), 545–568. https://doi.org/10.1016/j.rgg.2013.03.00.

Wall, F., Zaitsev, A.N., 2004. Phoscorites and carbonatites from mantle to mine: the key example of the Kola Alkaline Province. The Mineralogical Society Series. vol. 10. Black Bear Press, Cambridge.

Yarmolyuk, V.V., Bogatikov, O.A., Kovalenko, V.I., 2004. Late Cenozoic transcontinental structures and magmatism of the Earth's Euro-African segment and geodynamics of its formation. Dokl. Earth Sci. 395, 183–186.

Yu, J., Che, L., Wang, T., 2015. Alteration, oxygen isotope, and fluid inclusion study of the Meishan iron oxide-apatite deposit, SE China. Mineral. Deposita 50 (7), 847–869. https://doi.org/10.1007/s00126-015-0577-0.

Zaitsev, A., Bell, K., 1995. Sr and Nd isotope data of apatite, calcite and dolomite as indicators of source, and the relationships of phoscorites and carbonatites from the Kovdor massif, Kola peninsula, Russia. Contrib. Mineral. Petrol. 121 (3), 324–335. https://doi.org/10.1007/BF02688247.

Zaitsev, A.N., Wall, F., Bas, M.J.L., 1998. REE-Sr-Ba minerals from the Khibina carbonatites, Kola Peninsula, Russia: their mineralogy, paragenesis and evolution. Mineral. Mag. 62 (2), 225–250. https://doi.org/10.1180/002646198547594.